HHS Public Access

Author manuscript

Cell Rep. Author manuscript; available in PMC 2024 July 08.

Published in final edited form as:

Cell Rep. 2024 May 28; 43(5): 114144. doi:10.1016/j.celrep.2024.114144.

Prophylactic treatment with the c-Abl inhibitor, neurotinib, diminishes neuronal damage and the convulsive state in pilocarpine-induced mice

América Chandía-Cristi[1,7], **Daniela A. Gutiérrez**[1,2,7], **Andrés E. Dulcey**[3], **Marcelo Lara**[4], **Lina Vargas**[1], **Yi-Han Lin**[3], **Pablo Jimenez-Muñoz**[1], **Gabriela Larenas**[1], **Xin Xu**[3], **Amy Wang**[3], **Ashley Owens**[3], **Christopher Dextras**[3], **YuChi Chen**[3], **Claudio Pinto**[1], **Tamara Marín**[1,2], **Hugo Almarza-Salazar**[1,2], **Keryma Acevedo**[5], **Gonzalo I. Cancino**[1], **Xin Hu**[3], **Patricio Rojas**[4], **Marc Ferrer**[3], **Noel Southall**[3], **Mark J. Henderson**[3], **Silvana Zanlungo**[6,*], **Juan J. Marugan**[3,*], **Álvarez R Alejandra**[1,2,8,*]

[1]Department of Cellular and Molecular Biology, Pontificia Universidad Católica de Chile, Portugal 49, Santiago, Chile

[2]Millennium Institute on Immunology and Immunotherapy, Biological Sciences Faculty, Pontificia Universidad Católica de Chile, Portugal 49, Santiago, Chile

[3]Early Translation Branch, National Center for Advancing Translational Sciences (NCATS), NIH, 9800 Medical Center Drive, Rockville, MD, USA

[4]Neuroscience Laboratory, Biology and Chemistry Faculty, Universidad de Santiago de Chile, Avenue Libertador Bernardo O'Higgins, Santiago 3363, Chile

[5]Neurology Unit of Pediatric Division, Pontificia Universidad Católica de Chile, Avenue Libertador Bernardo O'Higgins 340, Santiago, Chile

[6]Department of Gastroenterology, Faculty of Medicine, Pontificia Universidad Católica de Chile, Avenue Libertador Bernardo O'Higgins 340, Santiago, Chile

[7]These authors contributed equally

[8]Lead contact

SUMMARY

*Correspondence: szanlungo@uc.cl (S.Z.), maruganj@mail.nih.gov (J.J.M.), aalvarer@uc.cl (A.Á.R.).

AUTHOR CONTRIBUTIONS

A.A.R., S.Z., and J.M. conceived and designed the experiments and, with D.A.G. and A.C.C., wrote the manuscript. A.C.C., L.M.V., C.P., T.M., and M.L. performed animal injection and diet experiments. L.M.V., M.L., C.P., A.C.C., G.L., H.A.S., and D.A.G. participated in the TLE studies and Racine's scale blind analysis. D.A.G., A.C.C., and G.I.C. performed and analyzed neuronal culture experiments. P.J.M. performed MTT assays. M.L. and P.R. performed electrophysiological recordings. C.D., Y.C., Y.H.L., A.O., M.F., and M.H. performed and analyzed *in vitro* assays for the development of neurotinib. A.M., X.X., and X.H. generated the neurotinib and c-Abl computational modeling. Illustrative-Science.com designed the graphical abstract.

SUPPLEMENTAL INFORMATION

Supplemental information can be found online at https://doi.org/10.1016/j.celrep.2024.114144.

DECLARATION OF INTERESTS

Neurotinib is under patent WO2019/173761 A1.

The molecular mechanisms underlying seizure generation remain elusive, yet they are crucial for developing effective treatments for epilepsy. The current study shows that inhibiting c-Abl tyrosine kinase prevents apoptosis, reduces dendritic spine loss, and maintains N-methyl-D-aspartate (NMDA) receptor subunit 2B (NR2B) phosphorylated in *in vitro* models of excitotoxicity. Pilocarpine-induced status epilepticus (SE) in mice promotes c-Abl phosphorylation, and disrupting c-Abl activity leads to fewer seizures, increases latency toward SE, and improved animal survival. Currently, clinically used c-Abl inhibitors are non-selective and have poor brain penetration. The allosteric c-Abl inhibitor, neurotinib, used here has favorable potency, selectivity, pharmacokinetics, and vastly improved brain penetration. Neurotinib-administered mice have fewer seizures and improved survival following pilocarpine-SE induction. Our findings reveal c-Abl kinase activation as a key factor in ictogenesis and highlight the impact of its inhibition in preventing the insurgence of epileptic-like seizures in rodents and humans.

Graphical abstract

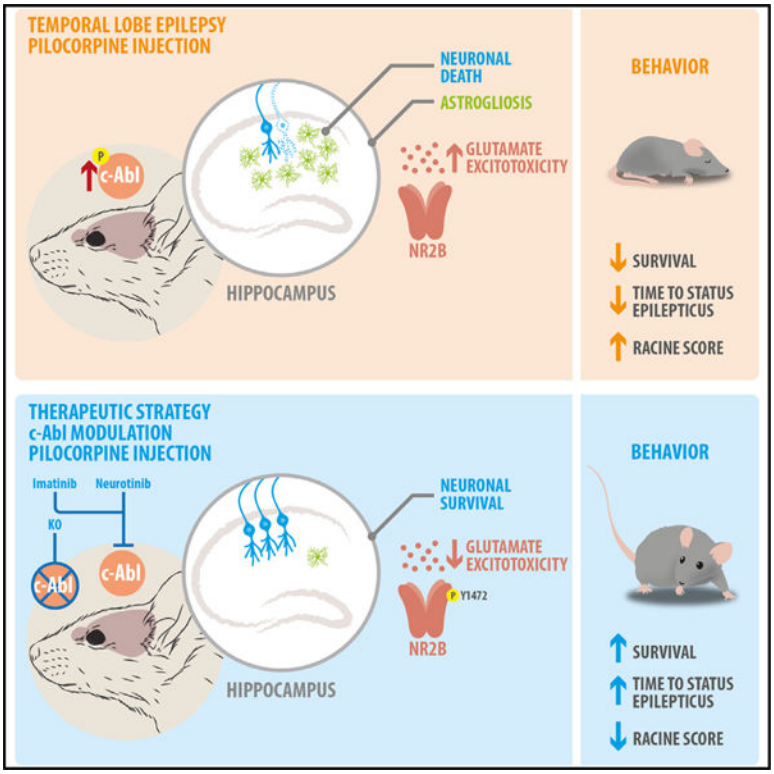

In brief

Chandía-Cristi et al. prove that the induction of acute seizures causes c-Abl protein phosphorylation. Importantly, they show that prophylactic treatment with c-Abl inhibitors, especially neurotinib, prevents the phosphorylation of c-Abl and the insurgence of epileptic-like seizures in mice. They further suggest the need to investigate neurotinib's translational potential in patients at high risk of developing epilepsy.

INTRODUCTION

Epilepsy is the fourth most common neurological disorder in the US, affecting around 50 million people worldwide (World Health Organization), and is characterized by recurrent seizures that interrupt normal brain function.[1,2] Recent studies suggest that 30%–40% of patients are resistant to commercially available antiepileptic drugs.[3–5] Temporal lobe epilepsy (TLE) is considered the most prevalent type among focal epilepsies and is defined by spontaneous seizures originating from the temporal lobe, mainly in the hippocampus and amygdala.[6,7] Patients with TLE show hyperexcitability of specific neuronal populations during ictogenesis (seizure generation),[8] which correlate with a decrease in dendritic spine density, aberrant axonal growth, cell death, and gliosis.[9,10] Similarly, Alzheimer ’s disease (AD) patients develop epileptiform activity due to alterations in parvalbumin interneurons, resulting in hippocampal hyperexcitability.[11,12] Indeed, increases in extracellular glutamate concentrations induce excitotoxicity and trigger the cellular events that promote seizures.[13–15] This signal is mediated by N-methyl-D-aspartate (NMDA) receptors (NMDARs), involved in the initiation and propagation of epileptic discharges, thereby promoting excitotoxic neuronal demise.[16,17] The NR2B-containing NMDARs have been linked to synaptic plasticity and excitotoxicity. NR2B overexpression improves synaptic plasticity and memory formation.[18] However, the NR2B and its Y1472 phosphorylated protein levels diminish after hippocampal seizures.[19] A misplace of receptors is often associated to leave the synaptic membrane,[20] excitotoxicity,[21–23] and decreased NMDAR-dependent currents, leading to memory and behavioral impairments and seizure development[24]

Although some cellular and molecular mechanisms involved in ictogenesis have been identified, there is a great need for new therapeutic approaches and targets for TLE. In this context, the ABL family of non-receptor tyrosine kinases (c-Abl or ABL1, and Arg or ABL2), are essential transducers of signals from growth factors, adhesion, and axon-guidance receptors, as well as stress response pathways.[25,26] c-Abl is highly expressed in neurons, especially in pre- and post-synaptic terminals. Compelling evidence places c-Abl as a regulator of neuronal homeostasis, synaptic plasticity, and gene expression after cognitive training.[27,28] However, c-Abl over-activation can be detrimental to neurons, being involved in the pathogenesis of several neurodegenerative diseases contributing to impaired mitochondrial function, oxidative stress, protein aggregation, and autophagy.[28–33] Inhibiting c-Abl improves neuronal outcome by reducing cell death, tau phosphorylation, dendritic spine loss, and cognitive impairments in animal models of AD,[34–36] further validated as a key factor for the hippocampal-spatial memory of APPSwe/PSEN1deltaE9 mice deficient in c-Abl activity.[37] Similarly, AD patients showed highly activated c-Abl associated to Aβ-peptide accumulation.[38] In epilepsy, a substantial increase in activated c-Abl has been reported in TLE patients and in pilocarpine-injected mice, where inhibiting c-Abl with imatinib has shown promising results as an anti-convulsing drug,[39,40] suggesting an important role for c-Abl in developing epilepsy. Marketed drugs that target Abl kinase activity are all orthosteric inhibitors that block the ATP-binding site of c-Abl (imatinib, dasatinib, nilotinib, bosutinib, and ponatinib) and were originally designed for the treatment of leukemia driven by a BCR-ABL fusion gene that produces a constitutively active kinase.[41] These drugs have limited central nervous system (CNS) penetration in comparison

with the levels in blood plasma and other tissues.[42–44] Among them, nilotinib showed slightly better ability to penetrate the blood-brain barrier (BBB).[45,46] However, as with other orthosteric c-Abl inhibitors, it targets additional kinases,[47] which can contribute to undesired side effects, such as those associated with an increased risk of stroke and other neurovascular events.[48–50] More selective, allosteric inhibitors, which bind to the myristoyl pocket of c-Abl[51] (e.g., GNF2), also have low CNS penetration. Thus, while the currently available c-Abl inhibitors are suitable tools for investigating the role of c-Abl in TLE *in vitro* and *in vivo*, they are not adequate for the treatment of TLE patients. Recently, we developed the c-Abl inhibitor neurotinib, which has been shown to be effective in Niemann-Pick A (NPA) and Alzheimer's mice models.[37,52]

Here, we show the contribution of c-Abl to the generation of epileptic seizures. c-Abl is activated in neurons exposed *in vitro* to excitotoxicity and in the mice brain after pilocarpine-induced status epilepticus (SE). Interestingly, genetic knockout of c-Abl or its inhibition can prevent cell death and decrease NR2B clustering upon excitotoxic damage. Using c-Abl knockout mice in the brain, and imatinib- or neurotinib-treated mice, we observed robust improvements in survival, resistance to seizures, and increased latency to SE. Neurotinib's good selectivity, CNS penetrability, and oral bioavailability showed promising therapeutic potential to prevent epileptic-like seizure development in patients.

RESULTS

c-Abl is activated by glutamate and NMDA-mediated excitotoxicity

To study the relationship between c-Abl and excitotoxicity, we exposed primary cultured neurons to 100 μM NMDA (Figure 1A) or 50 μM glutamate (Figure S1A). Activation of c-Abl, assessed by Y412 phosphorylation (p-c-Abl) status, significantly increase upon exposure to both NMDA and glutamate as early as 30 min post treatment, followed by a gradual decrease over a 4-h period. The peak activation of c-Abl (~1.5-fold) was observed at 30 min after both stressors, while total c-Abl levels remained unchanged (Figures 1A and 1B; Figure S1A). Additionally, NMDA exposure led to nuclear p-c-Abl localization and reduction of neuronal integrity, as shown by fluorescence using phalloidin staining (actin cytoskeleton), which was mitigated by c-Abl inhibition (Figure 1B).

Although early increases in total NR2B levels are observed after excitotoxicity or damage, the maintenance of phosphorylated levels of NMDAR, especially the 2B subunit at Y1472 (p-NR2B), have been associated with synaptic protection.[20,53] Here, the levels of p-NR2B strongly decreased in relation to the total NR2B subunit upon both NMDA and glutamate 4-h treatments (Figures 1C and S1B). Although non-significant, a trend was found for NR2B levels to increase after NMDA in comparison with glutamate treatments. To further establish that the effects observed are driven by c-Abl, we used neurons null for c-Abl, obtained from brain-specific knockout embryos (c-Abl-KO). Western blots showed NR2B levels partially increased mostly dependent on the 100 μM NMDA continuous exposure, not in genotype. c-Abl-KO neurons tend to maintain its p-NR2B levels when compared to wild type (WT), but non-significantly (Figure 1D). Overall, these results demonstrate that c-Abl is activated and seems to modulate NMDAR during neuronal excitotoxicity.

c-Abl kinase activity mediates cell death induced by excitotoxicity

To examine whether c-Abl activity is required for the induction of neuronal death by excitotoxicity, we exposed neurons to NMDA (Figures 2A and 2B) or glutamate (Figures S2A and S2B) for 24 h and measured cell viability using an MTT assay. We observed that both 100 μM NMDA and 50 μM glutamate induced a ~50% decrease in cellular viability. Neurons co-treated with imatinib (Figures 2A and S2A) or GNF2 (Figures 2B and S2B) displayed significantly higher viability across all tested NMDA and glutamate concentrations. We further investigated the impact of these inhibitors on neuronal apoptosis by evaluating nuclear Hoechst staining after a 1-h treatment with 100 μM NMDA. As expected, NMDA-induced excitotoxicity significantly increased the number of apoptotic nuclei. However, co-incubation of NMDA with either imatinib or GNF2 resulted in apoptosis reduction (Figures 2C and S2C). Additionally, c-Abl inhibitors preserved neuronal morphology in the face of NMDA exposure, as shown by βIII tubulin immunofluorescence, which was associated with a decrease in activated c-Abl (Figure 1C). Similarly, c-Abl-KO neurons showed a 14% reduction in apoptosis compared to WT neurons exposed to NMDA (Figure 2D). Even though the percentage of apoptotic nuclei is still higher than control neurons, c-Abl absence attenuates the apoptosis induced by 100 μM NMDA. Therefore, c-Abl inhibition or c-Abl genetic ablation protects against excitotoxicity induced by NMDA receptor agonists.

c-Abl inhibition or ablation prevents dendritic spine loss and NR2B expression changes in response to NMDA excitotoxicity

Excitotoxicity is associated with the loss of dendritic spines.[54,55] To evaluate c-Abl involvement in excitotoxicity-induced synaptic damage, we analyzed the morphology of GFP-expressing neurons and quantified dendritic spines. c-Abl inhibitors alone increased spine density at baseline, while 1-h NMDA treatment induced a significant decrease in spine density. However, when neurons were co-treated with c-Abl inhibitors, dendritic spine density was preserved, similarly to controls (Figure 2E).

Since excitotoxicity promotes an increase in total protein levels of NMDAR-NR2B,[53] we next analyzed NR2B subunit levels by immunofluorescence. NMDA excitotoxicity induced an increase in NR2B clustering. However, when neurons were pre-incubated with imatinib or GNF2, we observed less NR2B clustering (Figure 2F). The same result was obtained in c-Abl-KO neurons (Figure 2G). Thus, our results show that c-Abl is involved in excitotoxicity-induced dendritic spine loss and the regulation of NR2B clustering.

Neuronal c-Abl ablation increases survival and decreases seizure susceptibility after SE

To assess the participation of c-Abl during excitotoxic damage *in vivo* and to characterize the therapeutic potential of c-Abl inhibitors for epileptic seizures, we used pilocarpine-induced SE as a model for temporal lobe epilepsy (TLE)[56] (Figures 3A and S7A). Animal behavior was scored before and after presenting consecutive seizures, meaning that the animal has passed the orofacial seizures and maintains with uni- or bilateral forelimb clonus and/or presented tonic seizures, with or without rearing, stage 3–5 of Racine's scale, being in the convulsive state or SE; also, we recorded the time that animals took to reach the SE, here called ''latency to SE.'' Animals without SE were considered as 60-min latency

to SE. Stage 6 (death) of animal survival was also assessed.[57,58] First, we analyzed the effect of c-Abl inhibition on animal behavior, as seen in the summary table (Figure 3B and Table S1). When mice were intraperitoneally (i.p.) injected with pilocarpine, 97% of the vehicle-treated mice developed SE and only 3% developed seizures but not SE. Interestingly, 68% of mice pretreated with imatinib developed SE, while 29% developed seizures without reaching SE (Figures 3B and S7A). They also exhibited a longer latency to reach the convulsive state (vehicle = 16.9 ± 2.4 min; Ima = 30.7 ± 4.1 min) (Figures 3B and 3C). Furthermore, vehicle-injected animals had a high mortality of 69% in comparison with 36% in imatinib-injected mice (Figures 3B and 3E; Table S1).

A similar effect was observed when TLE mice were pretreated with GNF2 (Figure 3A). The percentage of mice injected with GNF2 that developed seizures significantly decreased to 11% (Figures 3B and S7B), while the latency was extended to approximately 55 min (vehicle = 18.6 ± 5.3 min; GNF2 = 55.3 ± 4.7 min) (Figures 3B and 3D). Furthermore, the mice exhibited improved survival, with 33% of them surviving (Figures 3B and 3F; Table S2), in comparison to the vehicle-injected group. c-Abl absence reduced the incidence of SE and mitigated the severity of acute seizures to 40% of animals exhibiting symptoms up to Racine scale 3, remaining in freezing (1), head nodding (2), or unilateral forelimb clonus (3). c-Abl-KO animals also showed increased latency to 36.2 ± 5.3 min compared to WT mice's 12.4 ± 1.7 min (Figure 4C) and significantly improved survival rates over WT counterparts (13% of c-Abl-KO vs. 64% of WT mice died) (Figures 4B and 4D; Table S3). Taken together, these results suggest that the ablation of c-Abl in the brain protects against seizure generation by reducing the severity and frequency of seizures in pilocarpine-induced SE animals, demonstrating a role for c-Abl in ictogenesis.

Increased excitability in the CA1 region during the latent period is assessed by a transient increase in the input-output field responses.[59] To further investigate the connection between c-Abl and circuit excitability in SE animals, we studied the evoked synaptic activity of CA3-CA1 circuit by stimulating Schaeffer's collateral and recording at *stratum radiatum* of hippocampal slices obtained from WT and c-Abl-KO mice after SE. Input-output (I-O) relationships were obtained by plotting the sEPSP slope in response to current stimulation ranging from 100 to 300 μA. The I-O curves between WT and c-Abl-KO mice did not differ (Figure 4E). In WT mice, the induction of seizures produced a left shift in I-O curves compared with their control littermates that did not undergo SE (Figure 4F). This curve shifting is consistent with an increase in excitability, as a product of plastic changes occurred during the SE.[60] In contrast, c-Abl-KO mice I-O curves did not change after pilocarpine-induced seizures and were similar to the non-treated WT and c-Abl-KO control mice (Figures 4G and 4H). Together, these results indicate that c-Abl deficiency protects the CA3-CA1 hippocampal circuit from short-term changes in excitability after SE, resulting in a decrease in seizure severity and increased survival.

Design and optimization of ABL1 allosteric inhibitors

We approached the design of improved allosteric c-Abl modulators by chemo-computational analysis of the GNF2-binding features in the myristoyl pocket,[61,62] followed up by an intense structure-activity-relationship (SAR) campaign. We explored and optimized

chemomimetics that satisfy binding requirements and display reasonable calculated medicinal chemistry properties to improve CNS penetration.[42–44,63,64] Following these premises, we obtained NCATS-SM1976, an allosteric c-Abl inhibitor hereinafter referred to as neurotinib[52] (Figure S3A).

Neurotinib docks into the myristoyl pocket of c-Abl in a similar manner to GNF2

To explore the potential binding interaction of neurotinib in c-Abl's myristoyl pocket, we used the published crystal structure of GNF2/c-Abl as starting point to perform a detailed comparative *in silico* docking analysis (Figure 5A). Two GNF2-binding models, with similar binding free energy, were predicted from an unbiased searching and docking using MOE Dock. The first binding model is the same as observed in the crystal structure, in which the amide group of GNF2 points to the left side of the myristoyl pocket and forms a water-mediated hydrogen bond (H-bond) in the solvent-exposed region (Figure 5B, magenta). In the second binding model, GNF2 amide group points to the right side by forming an H-bond with Glu481 (Figure 5B, dark green). Applying the same docking method and analysis, neurotinib showed similar right/left binding models to GNF2, modestly favoring the neurotinib's right-side binding mode, because the pyridine group points out and forms an H-bond with Glu481 (Figure 5C, green); the carbonyl group in the alternate configuration still forms a water-mediated H-bond in the inner pocket (Figure 5C, cyan). The overlaid docking structure of GNF2 and neurotinib show that both of them fit well into the myristoyl pocket, adopting similar binding models (Figures S3B and S3C). The tricycle core of neurotinib is quite flat (two aromatic rings joined together by a seven-member ring containing an amide group and an oxygen bridge) (Figure S3D) and is predicted form new water-mediated H-bonding interactions at the solvent-exposed region out of the myristoyl pocket.

Neurotinib binds and inhibits c-Abl in cells

To assess target engagement of neurotinib with c-Abl in cells, we developed a SplitLuc cellular thermal shift assay (CETSA).[65] Compound-induced thermal stabilization is not detectable for orthosteric or allosteric inhibitors of full-length c-Abl (Figure S4A) or BCR-ABL.[66] Thus, we created a reporter protein encoding a truncated c-Abl protein containing the kinase domain and myristoyl pocket. Cells heated up to 49°C caused 60% melt of the SplitLuc-c-Abl, GNF2 thermally stabilized c-Abl at single-digit micromolar concentrations; however, neurotinib did not (Figure 5D, supplementary file), indicating that these two molecules induce overall different global conformations within the selected construct. However, we predicted that neurotinib would compete with GNF2 and reduce GNF2-mediated thermal stabilization. When cells were exposed to neurotinib + 30 μM GNF2, neurotinib was able to compete and decrease, in a dose-response manner, the thermal shift induced by GNF2. At high concentrations of neurotinib, the thermal stability curve returned to vehicle control levels, completely outcompeting the effect of GNF2 (Figure 5E). Therefore, our results demonstrate that neurotinib displaces and eliminates the thermo-stabilizing effect in cell homogenates of an allosteric c-Abl inhibitor while not affecting the effect of an orthosteric molecule. To further evaluate neurotinib's binding to full-length WT c-Abl, we pulled down recombinant c-Abl protein with biotinylated inhibitors and streptavidin beads (Figure 5F). Biotiniylated-GNF2 retained recombinant c-Abl on the

beads,[51] while biotinylated neurotinib enhanced its enrichment, suggesting that neurotinib binds c-Abl more strongly than GNF2. Next, we performed neurotinib-GNF2 competition assays. Interestingly, while 0.2 μM GNF2 did not seem to displace c-Abl from biotin-GNF2 immobilized beads, the same concentration of neurotinib did. Either inhibitor at 2 μM displaced most of the c-Abl from the beads (Figure 5G). Together, these results indicate a strong binding of neurotinib to c-Abl myristoyl pocket, the same as GNF2.

To address neurotinib c-Abl inhibitory activity, we performed an *in vitro* phosphorylation assay incubating CRKII (a c-Abl cellular target)[67] GST-tagged and c-Abl immunoprecipitated from neurons treated with 100 μM H_2O_2. As controls, pre-incubation with imatinib and GNF2 inhibits CRKII-GST phosphorylation. As expected, neurotinib inhibited CRKII phosphorylation in the 0.1–1 μM concentration range (Figure 5H).

To address neurotinib c-Abl inhibitory activity, first we used K562 cells, proliferation of which depends on BCR-ABL activity. Neurotinib's half maximal inhibitory concentration (IC50) for K562 cells proliferation inhibition was ~2 μM (Figure S4B). We then probed neurotinib effect against 100 μM NMDA toxicity in neurons and found ~80% protection at neurotinib concentrations lower than 1 μM (Figure 5I). Increased concentrations of neurotinib reduced c-Abl phosphorylation and the activation of CRKII (Figure 5J). Interestingly, when c-Abl-KO cells were incubated with neurotinib, NMDA excitotoxicity significantly induced neuronal apoptosis, suggesting toxicity in c-Abl absence (Figure S4C). This indicated that neurotinib could modulate c-Abl function and exerts a protective effect in cells.

Neurotinib displays improved selectivity and CNS pharmacokinetics in comparison to other c-Abl inhibitors

Allosteric kinase inhibitors are usually much more selective than orthosteric inhibitors. Indeed, GNF2 has been described as a non-competitive inhibitor that selectively targets the ABL family.[47] Neurotinib proved to be highly selective when evaluated in two kinase selectivity profiling panels (Eurofins and Reaction Biology).

Since existing c-Abl inhibitors display variable BBB penetrance,[42–44,63,64] we performed multiple studies analyzing the pharmacokinetic properties of neurotinib compared to imatinib, nilotinib, and GNF2. Compound exposure in the brain (Figure 5K) and plasma (Figure 5L) upon a single-dose i.p. administration at 12.5 mg/kg of these c-Abl modulators was examined. Administration of GNF2 at a dose of 12.5 mg/kg induced severe *in vivo* toxicity within a few hours but was tolerated at 5 mg/kg, with no toxicity observed. Neurotinib brain exposure and half-life in the brain (t_{iv} ½ = 11 to t_{IP} ½ = 23 h, sheet 5 data file) were much greater than imatinib, nilotinib, or GNF2 (Figure 5M). Additional pharmacokinetic studies disclosed that neurotinib has high bioavailability (Figure S5A), with preferential distribution toward brain upon oral or intraperitoneal administration.

To evaluate the feasibility of oral and chronic use of neurotinib, we pursued the administration of neurotinib, nilotinib, and imatinib through diet and carried out pharmacokinetic studies to measure the exposure levels at 14 days. Chow containing 20, 67, or 200 ppm was expected to provide daily exposure to each inhibitor equivalent to 3, 10,

and 20 mg/kg, respectively. No signs of acute toxicity or changes in behavior were observed during the duration of the studies. The 14-day administration of neurotinib-containing diets yielded considerably higher brain exposure levels than nilotinib- and imatinib-containing diets at equivalent concentrations (Figure 5J). In addition, while nilotinib and imatinib display a low brain/plasma distribution ratio, neurotinib displays a high brain/plasma ratio, indicating preferential distribution of neurotinib toward the CNS, in alignment with previously described i.p. and oral pharmacokinetic studies (supplementary data file). Taken together, these results indicate that neurotinib is a selective inhibitor of c-Abl with enhanced tolerability and BBB penetrance compared to known orthosteric and allosteric c-Abl inhibitors.

Neurotinib inhibits the increase in c-Abl phosphorylation in pilocarpine-induced SE mice, protecting mice against seizures and improving survival

Next, we evaluated neurotinib in pilocarpine-induced seizures as a model for TLE. First, 6-week-old mice were daily injected with either vehicle or neurotinib (5 mg/kg) for 3 days (Figure 6A). On the third day, SE was induced with pilocarpine, and 95% of vehicle-treated mice developed the SE (Figure 6B) with 17 ± 2.6-min latency (Figure 6C). Interestingly, only 54% of neurotinib-pretreated mice developed the SE (Figures 6B and S7C; Table S4) with significantly higher latency (39.2 ± 5.7 min) (Figure 6C). Likewise, neurotinib significantly improved mice's survival to 62% compared to vehicle-injected mice, which exhibited 38% survival (Figure 6D). To validate the c-Abl inhibition in neurotinib-treated animals, we performed immunohistochemistry of coronal brain sections (Figure 6E) and western-blot analyses of hippocampal tissues (Figures 6F and 6G) of neurotinib-i.p.-injected animals that survived after SE induction. We found that c-Abl phosphorylates in Y412 in pilocarpine-injected animals and 3-day neurotinib injection decreased p-c-Abl levels, inhibiting c-Abl activation (vehicle vs. pilocarpine, $^{**}p = 0.0032$; pilocarpine vs. neurotinib + pilocarpine $^{*}p = 0.0191$).

To minimize the stress associated with daily i.p. administration,[68] we repeated the pilocarpine-induced SE studies with neurotinib delivered *ad libitum* access to chow as soon as animals started solid diet (67 ppm, providing a 12.5 mg/kg daily ingestion dose; Figure 7A) for 15 days. We used nilotinib as another orthosteric c-Abl inhibitor for comparison, as its clinical use is vastly reported.[43,44,49] As before, we followed the SE onset according to Racine's scale, over 60 min (Figure S7D). In this study, 100% of control-diet-fed mice developed seizures after pilocarpine injection (Figure 7B) and reached SE with a latency of ~14 min (Figures 6B and 6C; Table S5). In contrast, 67% of neurotinib-fed mice, and 70% of nilotinib-fed mice developed SE (Figure 6B) and showed significantly longer latency compared to control fed mice (vehicle diet = 13.8 ± 1.5 min, neurotinib diet = 36.7 ± 6.3 min, nilotinib diet = 32.6 ± 6.1 min) (Figure 6C). Furthermore, none of neurotinib- and nilotinib-fed mice died (Figure 6D).

The TLE model display neuronal loss and astrogliosis after 24 h of seizure induction.[69] We evaluated astrocytes (GFAP), and neuronal (NeuN) populations by immunofluorescence in the hippocampus of neurotinib-fed mice. Since mice were sacrificed only 1 h after SE, they

did not develop epileptogenesis. Thus, as expected, we found no astrogliosis or neuronal loss after an hour of seizure induction (Figure S6).

c-Abl inhibition normalizes phosphorylation of the NMDA receptor NR2B subunit in SE animals

To evaluate if this seizure protection is related to NMDAR-NR2B phosphorylation, we compared the levels of p-NR2B Y1472 in hippocampal tissues from untreated vs. GNF2 or neurotinib-treated SE mice. We found a trend toward reduced p-NR2B levels in hippocampal tissues in the SE mice by western blot. When SE mice were treated with the allosteric inhibitor GNF2 (Figures 3G–3I), p-NR2B levels were preserved. Like GNF2, the same trend was found in i.p.-injected neurotinib animals (Figures 6F–6H), and neurotinib-fed animals (Figures 7E–7G) after pilocarpine injection, while NR2B total levels were variable among conditions but seemed to remain low with c-Abl inhibitors after pilocarpine. These results suggest that c-Abl allosteric inhibition helps to maintain the levels of phosphorylated NR2B subunits after TLE induction.

To evaluate the potential off-target activity of neurotinib, we administered the diet containing neurotinib (67 ppm) to WT and c-Abl-KO mice for 15 days prior to pilocarpine injection (Figure 7H). Similar to neurotinib-i.p. mice, WT mice fed with neurotinib diet were protected against pilocarpine-induced seizures, showing longer latency and complete survival compared to control normal-diet WT mice. Interestingly, neurotinib had a detrimental effect in c-Abl-deficient animals. Indeed, all WT-control-diet- and c-Abl-KO-neurotinib-fed mice developed the SE, while only 57% of c-Abl-KO mice did (Figure 7I). In accordance, cAbl-KO mice fed with neurotinib diet showed a shortened latency (WT-neurotinib diet = 32.3 ± 7, c-Abl-KO-neurotinib diet = 15.9 ± 3 min) (Figures 7I and 7J; Table S6) and did not have an improved life span (Figure 7K). These results indicate that the protective effects of neurotinib in the mouse model of SE depend on c-Abl expression. Moreover, they also suggest that neurotinib might act as a stressor in the absence of c-Abl.

Neurotinib ameliorates the convulsive state in kainic-acid-induced SE mice

To further investigate the contribution of c-Abl in regulating seizure susceptibility *in vivo*, we used another model to chemically induce acute seizures based on the administration of a neuro-excitatory glutamatergic agonist, kainic acid (KA).[70] After KA injection, we observed the SE on WT, c-Abl-KO, and WT neurotinib-fed animals for 2 h. All displayed motor seizures (Figure 7L) within the first 15 min and peaked approximately 60–90 min after KA injection (30 mg/kg) (Figures 7M–7Q). However the seizure profile (i.e., seizure score distribution) was significantly different in c-Abl-KO mice and WT neurotinib-fed mice compared to WTs (Figures 7M and 7N). Both groups had lower accumulative score than KA-treated WT mice (Figure 7O). Interestingly, c-Abl inhibition or ablation notably affected the median seizure activity scores (Figure 7P). Also, the latency to develop SE, clonus, and death increased almost three times in c-Abl-KO and WT-neurotinib-fed mice compared to WT mice (WT = 35.14 ± 6.17; c-Abl-KO = 94.86 ± 15.83; WT-neurotinib = 59 ± 13.81 min) (Figure 7Q). Therefore, our results showed that the absence or inhibition of c-Abl delayed seizure susceptibility in the KA model of SE, further validating c-Abl as a molecular target for ictogenesis.

Altogether, our results indicate that neurotinib prevents the induction of epileptic seizures in mice, validating this molecule as a preclinical candidate to develop new treatments for seizure disorders and especially in patients at high risk of developing future epileptic-like seizures.

DISCUSSION

The lack of pharmacological targets for epileptogenesis, knowledge for ictogenesis, and the failure of these drugs to reach their targets in the brain[3,5,71] make TLE the most challenging epilepsy to treat.

Here, we describe the activation of the non-receptor tyrosine kinase c-Abl in response to glutamatergic excitotoxic damage in cultured neurons as a key mechanism that mediates the pathological features associated with seizure susceptibility in a pilocarpine-induced SE mouse model.

Current US Food and Drug Administration (FDA)-approved c-Abl inhibitors have numerous limitations impairing their practical use to treat CNS disorders. In general, orthosteric kinase inhibitors display poor on-target selectivity, targeting Arg, c-kit, and PDGFR besides c-Abl.[47] Among the approved, nilotinib is among the most selective.[47] GNF2, however, is non-FDA approved and is quite selective, targeting only the ABL family, but it suffers from limited CNS penetration.[50,63,64] Using the published crystal structure of GNF2/c-Abl as a starting point to perform a detailed comparative *in silico* docking analysis,[51,61,62] we designed neurotinib, with improved pharmacological properties, which has already showed promising effects on NPA and AD models.[37,52] We show that neurotinib binds c-Abl more strongly than GNF2, providing experimental support for binding in the myristoyl pocket. Moreover, *in vitro* phosphorylation assays showed that neurotinib inhibits the phosphorylation of the classic c-Abl substrate, CRKII, proving that neurotinib binds and inhibits c-Abl kinase activity. Importantly, neurotinib displays good oral bioavailability and *in vivo* tolerability, excellent once-a-day pharmacokinetics, and preferential distribution toward the CNS (Figure 5), a major hurdle of the previously described c-Abl inhibitors.

Recently, several human clinical trials studying the effects of nilotinib as a potential treatment for AD and Parkinson’s disease (PD) have been carried out. Nilotinib was selected because of its high potency toward c-Abl, reasonable selectivity, and better CNS exposure than the rest of the FDA-approved c-Abl inhibitors. However, the results of PD phase II human clinical trials have been disappointing, with no clear improvement, most likely as result of its poor brain penetration (0.2%–0.3%) in humans.[44] Mixed results were observed with nilotinib in AD patients at the maximum tolerated 300-mg daily dose despite displaying 2–4 nM nilotinib in CSF,[43] levels enough to reduce the Aβ burden in the brain. Our in-house pharmacokinetic studies confirmed the low capacity of nilotinib and other c-Abl inhibitors to penetrate the BBB. In contrast, neurotinib yields high concentration levels in CNS upon administration at a reasonable dose of 12.5 mg/kg, allometrically equivalent to 1 mg/kg in human subjects[72] (Figure 5).

Recently, Singh's group[40] employed the pilocarpine model at a sub-convulsive dose of 100 mg/kg (i.p.) every third day per 31 days to investigate the role of c-Abl in the pathogenesis after SE. c-Abl expression was increased in mice during pilocarpine-induced spontaneous seizures (epileptogenesis), validating imatinib as an antiepileptic drug. Similarly, we have described here that imatinib, GNF2, nilotinib, and neurotinib reduced the susceptibility for developing SE while maintaining mice in a less severe convulsive state. This supports the idea that c-Abl inhibitors work as anti-convulsing drugs. Imatinib was applied at 1 and 3 mg/kg starting at day 6 of the experiment, while, in our model, 12.5 mg/kg imatinib and 5 mg/kg neurotinib were applied for 3 days before pilocarpine, supporting that these inhibitors work during the ictogenesis phase of epilepsy.

The i.p. injection route can add stress to animals and lower their survival rate,[68] which is already low in pilocarpine models.[73] Thus, we focused on developing an oral delivery of neurotinib to properly evaluate the effect of c-Abl in seizure generation and further translational future. Our chow doses were equivalent to 10.0 mg/kg total daily dose, yielding nearly micromolar levels in the brain throughout the day. In the treatment group, only half of the animals developed SE compared to regular food. c-Abl-KO mice fed neurotinib were not as protected as WT-control-diet mice were against pilocarpine-induced SE, validating the on-target activity of the molecule. We did not observe any abnormalities or changes in behavior upon long-term exposure of WT animals to neurotinib (Figures 6 and 7). Interestingly, the same effect was observed in c-Abl-KO cultured neurons treated with neurotinib and exposed to NMDA damage, further demonstrating that neurotinib acts as a neuronal stressor in c-Abl absence (Figure S4C), and its neuroprotective activity in WT neurons is c-Abl dependent.

Although a nilotinib diet also showed protection against pilocarpine-induced seizures, there were significant differences in dose and levels of CNS exposure between neurotinib and nilotinib. The highest daily amount we used for nilotinib-supplemented diet was 200 ppm, exposing the animals to an equivalent daily dose of 30 mg/kg, allometrically equivalent to 2.4 mg/kg in humans, being in the range of recently used concentrations for PD human clinical trials, which further show nilotinib safety at 300 mg.[45,46]. Previous efficacy studies in mouse models of PD using daily oral gavage administration of nilotinib at 25 mg/kg yielded 7 pg/mg of nilotinib in the brain (13.2 nmol/kg) and showed robust protection of dopaminergic neurons and amelioration of disease phenotype.[74] However, allometric scaling of this dose into human clinical trials failed to recapitulate these results in PD patients, pointing to a poor alignment between human and mouse models. In our efficacy studies, neurotinib diet was 67 ppm, equivalent to one-third of nilotinib dose, and in the range of 10 mg/kg yields high and preferential distribution toward the brain, including much higher levels in CNS when compared to nilotinib. Concerning the molecular targets of c-Abl during ictogenesis, it has been discussed that NMDARs play a major role in the generation of seizures and excitotoxicity.[16,75–77] They promote aberrant epileptic circuits that, in a vicious cycle, can cause spontaneous seizures whose frequency and severity worsen brain damage.[10,78] The NR2B subunit can be regulated by multiple kinases. In particular, Fyn facilitates NR2B-NMDAR's interaction with the post-synaptic density (PSD),[19,79] c-Abl regulates the clustering of the PSD protein PSD95,[80] and the NR2D subunit of NMDAR inhibits c-Abl auto-phosphorylation.[81] Thus, c-Abl could be participating in the

regulation of seizure susceptibility by modulating NR2B levels and affecting the population of dendritic spines, promoting synaptic plasticity changes in response to seizures. Using RNA sequencing (RNA-seq) analysis, our grouped showed that c-Abl deficiency in the nervous system promotes a transcriptional program that affects the synapse.[27] Genes such as *Atad1*, encoding the Thorase protein; AMPAR regulator; and Arp2/3, which promotes actin polymerization for dendritic spine morphology changes are upregulated in c-Abl-KO mice after learning in mice. Enhanced learning by c-Abl deficiency could be the result of increased mushroom dendritic spine density, the most mature form of spines, which are enriched in receptors.[27] As we also saw in culture, dendritic spine density is basally increased in the absence of c-Abl, enriched in both mature and immature spines, with population displacement after Aβ-oligomer incubation (*in vitro* model for early-AD).[36] Furthermore, current results demonstrate that dendritic spine density is preserved after NMDA treatment, and toxic clustering of NR2B is reduced when co-incubated with c-Abl inhibitors. Therefore, c-Abl seems to be modulating NMDAR after seizure induction.

Increases in c-Abl phosphorylation have become a common factor in the development of neurodegenerative diseases such as AD.[31–33,37] Chen's group showed that patients with TLE and pilocarpine-treated rats had increased total c-Abl after 6 h of seizure induction and high p-c-Abl levels in the temporal neocortex maintained up to 60 days.[39] This experiment suggests that c-Abl responses to induced seizures could be modulating neurons. In our SE mice, c-Abl phosphorylates during the hour of seizure induction, in a generalized expression pattern along the brain cortex and hippocampus that is inhibited by neurotinib (Figure 6), delaying ictogenesis.

Overall, this study sheds light on the molecular mechanisms underlying seizure generation and highlights the potential of targeting c-Abl kinase with neurotinib as preventive treatment for patients with high risk of developing seizure-like conditions. Further research and clinical trials will be needed to validate these findings and assess the full therapeutic potential of neurotinib.

Limitations of the study

Although, in *in vitro* experiments, c-Abl phosphorylation increases under pathological conditions and c-Abl-KO neurons displayed less apoptosis than WT neurons after NMDA exposure, the percentage of apoptotic cells remained higher than controls, suggesting that other NMDA-induced apoptotic signaling pathways are contributing to neuronal excitotoxicity, which requires further research.

Moving to *in vivo* studies, the administration of c-Abl inhibitors via i.p. injection in mice, as part of daily manipulation, introduced stressors that affected neurotinib's protective effects. Despite these initial promising outcomes, a comprehensive assessment of neurotinib's safety and long-term tolerability through systematic studies is necessary before considering translation to human patients.

STAR★METHODS

RESOURCE AVAILABILITY

Lead contact—Further information and requests for resources and reagents should be directed to and will be fulfilled by the lead contact, Alejandra Álvarez Rojas (aalvarez@bio.puc.cl).

Materials availability—There are restrictions to the availability of neurotinib due to patent WO2019/173761 A1.

Data and code availability—Original western blot images and Raw data [Excel file] have been deposited at Figshare and are publicly available as of the date of publication. Accession numbers are listed in the key resources table (http://figshare.com/s/d460eb722b56b5075fcd). Microscopy data reported in this paper will be shared by the lead contact upon request. This paper does not report original code. Any additional information required to reanalyze the data reported in this paper is available from the lead contact upon request.

EXPERIMENTAL MODEL AND STUDY PARTICIPANT DETAILS

Animal care and use—Pregnant Sprague–Dawley rat (RRID:MGI:5651135) at embryonic day 18 (E18), C57BL/6J (RRID:IMSR_JAX:000664) and c-Abl knockout (cAbl-KO) mice were maintained in the Animal Care Facility of Pontificia Universidad Católica de Chile (CINBIOT). c-Abl null mice were bred from B6.129S4-Abl1tm1Ajk/J (*loxP* sites in Abl1 exon 5, RRID:IMSR_JAX:024286) x B6.Cg-Tg(Nes-cre)1Kln/J (RRID:IMSR_JAX:003771). Therefore, only neuronal and glial progenitor cells will lack c-Abl.[27] Genotyping of c-Abl-KO mice was performed using a PCR-based screening according to Jackson's protocol 31758 for Nes-Cre in Chr12 (Primers: WT-Fw: TTGCTAAAGCGCTACATAGGA; Common: GCCTTATTGTGGAAGGACTG; Tg-Fw: CCTTCCTGAAGCAGTAGAGCA). This study used 5-week-old male C57BL/6J and cAbl-KO mice for SE induction. All procedures were approved by the ad hoc committee of Chile (ANID) and the Institutional Animal Care and Bioethical and Biosafety Committee of the UC (Protocol #190610036, #210302001), also by the National Center for Advancing Translational Sciences, (NCATS), National Institutes of Health (NIH).

Cell lines—K562 (ATCC: CCL-243) and HEK293 (RRID:CVCL_0045) cells were seeded onto poly-L-lysine-coated plates (0.5 mg/mL), grown in DMEM high glucose supplemented with 10% FBS, and maintained at 37°C in 5% CO_2.

Primary neuronal culture—The hippocampi and brain cortex were pooled among 10 to 18 embryos (depending on pregnancy) from the same pregnant Sprague–Dawley rat at embryonic day 18 (E18). Only when c-Abl-KO neurons were used, two hippocampi and two brain cortices (one from each hemisphere) were pooled together without mixing with other embryo's tissue as each embryo can be wild-type or conditional KO for c-Abl. Cultures were prepared as before.[83] Briefly, tissue was re-suspended in HBSS containing 0.25% trypsin, incubated 20 min at 37°C, and rinsed 3x HBSS. Then, tissue was mechanically

dissociated and neurons re-suspended in DMEM supplemented with 5% horse serum and seeded onto poly-L-lysine-coated plates (0.5 mg/mL). Cultures were maintained at 37°C in 5% CO_2 and after 4-h culture medium was replaced with Neurobasal supplemented with 2% B27, 2 mM glutamine, 100 U/ml penicillin, and 100 μg/mL streptomycin. Proliferation of non-neuronal cells was limited using cytosine arabinoside 1 μM.

METHOD DETAILS

Neuron transfection—At 15 DIV (days *in vitro*), neurons were transfected using the Magnetofection technology (Oz Biosciences), using GFP expression plasmids for morphology analysis.

Pilocarpine induced status epilepticus (SE)—As reported,[73] the status epilepticus was induced in 5-week-old male C57BL/6J or c-Abl conditional knockout male mice by a single intraperitoneal (IP) injection of 420 mg/kg pilocarpine hydrochloride (Sigma-Aldrich P6503). First, mice were administered scopolamine methyl nitrate IP to block the peripheral muscarinic effects of pilocarpine: 1.5 mg/kg (Sigma-Aldrich S2250) 15 min before pilocarpine injection to inhibit the peripheral cholinergic effects. 45 min after injection of pilocarpine, diazepam was injected IP at 15 mg/kg (Sigma-Aldrich D0899) to halt convulsions. Behavioral seizure activity was documented immediately after pilocarpine injection by an investigator blind to experimental conditions using the modified Racine's stages[57,58] (0 = no seizures; 1 = freezing, secretions; 2 = orofacial seizures, single twitches, head nodding, 3 = unilateral forelimb clonus, paralysis; 4 = bilateral forelimb clonus without rearing; 5 = tonic/clonic seizures, loss of posture, bilateral forelimb clonus with rearing; and 6 = death). Control groups were administered with scopolamine methyl nitrate, diazepam, and vehicle (saline solution). Every experimental set included a vehicle and drug treatment group for each c-Abl inhibitor used. Data was then pooled, not randomized and analyzed as a whole.

Kainic acid: Kainic acid was given in a single IP dose of 30 mg/kg (Andres Dulcey laboratory, NIH, USA) dissolved in saline. WT and c-Abl-KO mice were evaluated at eight-week-old. WT mice of three-week-old were fed with neurotinib (67ppm) *ad libitum* for five-week-old. Seizures were recorded by a video cam and scored according to previously described criteria.

c-Abl inhibitors treatment—For animal experiments, mice received daily intraperitoneal injections of imatinib mesylate (Novartis, Basel, Switzerland) 12.5 mg/kg in 0.9% NaCl or GNF2 (Sigma-Aldrich G9420) 5 mg/kg in 0.9% NaCl or neurotinib (synthesis in supplementary materials) 5 mg/kg in 0.9% NaCl for 3 days. Control groups (vehicle) received daily intraperitoneal injections of 0.9% NaCl. Pilocarpine was injected 30 min after the third injection of c-Abl inhibitors. In diet experiments, 3-week-old (21 days) male mice were fed with control food, neurotinib (67 ppm) *ad libitum* as soon as weaned for 15 days. Rodent chow was manufactured by Envigo/Teklad by incorporation of neurotinib ppm or nilotinib (200 ppm) into the NIH-31 Open Formula Mouse/Rat Sterilizabile Diet (7017), followed by irradiation handling of the final product. *In vitro*, hippocampal and cortical

neurons were pre-treated with 5 μM imatinib or GNF2 for apoptotic nuclei, dendritic spine and NR2B cluster quantification.

Tissue distribution and pharmacokinetic study—Male mice were divided into 3 groups of increasing dose concentration (n = 3 mice/point): 3, 10 and 30 mg/kg of neurotinib, imatinib, and nilotinib administered in mice diet at approximately 3g/mouse/day during 15-day administration. Plasma, liver and brain were collected at different time points: 4, 8, 12, 16, 20, 24 h post dose after the last dose at the 15th day (n = 3 animals/time point). Brain and liver samples were obtained after mice were fully exsanguinated, weighted before analysis, and homogenated. Plasma samples (approximately 0.2 mL) were collected by cardiac puncture at each time point and placed into Heparin-Na collection tubes before centrifugation (4.000 g × 5 min, 4°C) to obtain plasma. Bioanalysis was performed by Pharmaron.

Cytotoxicity assays—Cortical neurons were seeded in poly-L-lysine-coated 96-well plates at $1x10^5$ cells/100 μL per well and maintained in Neurobasal medium supplemented with B27 for 7 DIV. Then, neurons were deprived of B27 and treated with 10–100 μM L-glutamic acid (glutamate, Sigma G2128), and NMDA (Tocris 0114) with or without the c-Abl kinase inhibitors (imatinib, GNF2 or neurotinib). After a 24-h incubation, cell viability was measured by the modified 3-[4,5-dimethylthiazol-2-yl]-2,5-diphenyltetrazolium bromide (MTT) assay.[82] The same assay was used in K562 cells. After 72-h incubation with c-Abl inhibitors, the IC50 was measured for each drug.

Cloning—A C terminus 86b acceptor backbone was created as previously described,[65] with the 86b tag encoding Gly-Ser-HiBiT-Gly-Ser. A gene strand encoding the kinase domain of c-Abl (aa 229–512; NP_005148.2) was synthesized by Eurofins and cloned into the NheI and BamHI sites of the acceptor backbone using InFusion reagents (Takara), to create an c-Abl-86b fusion protein. The coding region was sequence confirmed (Eurofins).

CETSA target engagement assay—Hek293 (ATCC CRL-1573) cells were transiently transfected by adding 22.5 μg of plasmid and 45 μL of Lipofectamine 2000 in 9 mL OptiMEM to a T75 flask. Then 10 million cells suspended in 3 mL of DMEM containing high glucose and 1X glutamax with 10% FBS were added to the transfection complexes. After 24 h, cells were lifted with 0.25% trypsin and resuspended to 1 million cells/ml in phenol free DMEM with high glucose and 1X glutamax. Cells were treated with 30 μM GNF2 in bulk then 10 mL of cells was dispensed into 384-well PCR plates using a Multidrop Combi. 52 nL of DMSO or compound was pinned into the plates then incubated for an hour at 37°C. The plates were then heated to 49°C for 3.5 min in a thermal cycler, cooled to RT, and lysed with NP40 and protease inhibitors for 30 min. Following lysis, 5 μL of substrate was added (0.33X furimazine, 100 nM of the 11s large fragment). Luminescence was then detected using a PerkinElmer ViewLux microplate reader equipped with clear filters.

Abl pulldown and inhibitor competition—0.5 μg recombinant human c-Abl protein (ThermoFisher Scientific, PR4348B) was incubated with 20 μL M-280 Streptavidin Dynabeads (Invitrogen, 11205D) immobilized with biotinylated GNF2 or neurotinib. The

sample was incubated at 4°C with rotation for an hour. The beads were washed three times with PBS (pH 7.4) containing 0.01% Tween 20 (PBST) and re-suspended in 40 μL Laemmli buffer. After incubating at 70°C for 5 min, the bound c-Abl protein was resolved on an SDS-PAGE and analyzed by an α-His tag (Invitrogen, MA1–21315) immunoblot. Competition assay was performed by adding 0.5 μg recombinant c-Abl protein, pre-incubated with GNF2 or neurotinib at indicated concentrations at 4°C for 30 min, to 20 μL M-280 Streptavidin Dynabeads immobilized with biotinylated GNF2. The sample was incubated at 4°C with rotation for 30 min. The beads were washed with PBST, re-suspended in Laemmli buffer, and analyzed by an α-His tag immunoblot.

***In vitro* phophorylation kinase assay—**Kinase assay mixtures contained 25 mM HEPES pH 7.25, 100 mM NaCl, 5 mM $MgCl_2$, 5% glycerol, 100 ng/μL bovine serum albumin, 1 mM Na_3VO_4, CRKII-GST, and 1 mM ATP. Activated c-Abl was immunoprecipitated with 4 μg c-Abl 24–11 antibody (SCT) from neurons treated for 15 min with 100 μM hydrogen peroxide (H_2O_2) and lysed in low-detergent buffer. Proteins were quantified and 1000–500 μg of the lysate were used for the assay. Recombinant CRKII was purified from GST bacteria with Streptavidin beads and glutathione. Negative control for c-Abl phosphorylation of CRKII-GST consisted on the substrate diluted on ATP buffer. c-Abl inhibitors were incubated for 20 min at RT with the enzyme prior the addition of the CRKII-GST substrate. Neurotinib ranged 10–0.1 μM, 5 μM of imatinib and GNF-2. Kinase mixtures were then incubated for 60–40 min at 30°C, then re-suspended in Laemmli buffer. Tyrosine phosphorylation was evaluated by western-blot using an anti-phospho-tyrosine (*p*-Tyr) antibody 4G10 (Millipore).

Immunoblot—Primary neuronal cultures and brain samples were extracted using RIPA buffer (25 mM Tris-HCl pH 7.6, 150 mM NaCl, 1% NP-40, 1% sodium deoxycholate, 0.1% SDS) supplemented with protease inhibitors (1 mM Na_3VO_4, 1 mM NaF, 1 mM PMSF, 1 μg/mL Pepstatin and 1 μg/mL Aprotinin and 1 μg/ml leupeptin) at 4°C. Then, lysates were centrifuged at 14.000 rpm at 4°C for 10 min. And protein concentration was assessed with BCA Protein Assay kit (Thermo Fisher Scientific, USA). Proteins were resolved in SDS PAGE and transferred to nitrocellulose membranes. Membranes were blocked in 3% BSA-0.1%-TBST at RT for 1-h and specific primary antibodies were used for O/N incubation at 4°C. At the next day, membranes were washed and incubated with corresponding HRP-secondary antibodies in 3% BSA-0.1% TBST for 1-h at RT. Primary antibodies used: anti-phospho-NR2B (Y1472) (38–7000; Thermo Fisher Scientific), anti-NR2B (75–101; Neuromab), anti-phospho-*c*-Abl (Y412) (C5240; Sigma-Aldrich), anti-*c*-Abl (A5844; Sigma-Aldrich, USA), anti-GAPDH (6C5) (sc32233) and anti-β3 Tubulin (2G10) (sc80005).

Fluorescence and DAB labeling—Cells were washed with 1X PBS, fixed in 4% PFA/PBS for 20 min, washed with 1X PBS and permeabilized for 10 min in 0.2% Triton X-100 in PBS. After 2 washes with PBS, cells were incubated in 3% BSA-PBS for 40 min at RT, followed by an O/N incubation at 4°C with primary antibodies (same antibodies used for immunoblotting). The cells were washed with PBS and incubated with Alexa-Fluor secondary antibodies for 1-h at RT. To quantify the apoptotic nuclei population, the neuronal

nucleus was labeled with Hoechst 33342 staining, during the incubation of the secondary antibody. Images were captured with a Zeiss LSM 5 Pascal or Nikon Eclipse C2 Ti-E confocal microscope and analyzed with ImageJ software.

Mice brains were cut into 30 μm slices (cryostat Leica CM1850). For immunofluorescence 2–3 slices were washed three times in PBS. Then subjected to successive incubations of 0.4% Triton X-100, 0.15 M glycine, and 50 mM $NaHBO_4$ solutions. Washed three times in PBS 1x and incubated with blocking solution (0.4% Triton X-100 with 3% BSA in PBS 1x) for an hour before primary antibody incubation O/N at 4°C (GFAP 1:600 Cell signaling 3679; Iba1 1:300 Novus Bio NB100–1028; NeuN 1:1000 Abcam #177487). The next day brain slices were washed three times with PBS 1x for 15 min each, and incubated with secondary Alexa Fluor antibodies for an hour at RT. Finally, brain slices were washes two times with PBS 1x, incubated with Hoechst, and mounted into coverslips for microscope visualization. For immunohistochemistry, slices were treated with H_2O_2 0.3% for 30 min, washed four times with PBS, treated with NaBH4 10 mg/mL for 15 min, washed with PBS three times by 10 min, and blocked with BSA 0.5% Triton X-100 0.2% for 1 h. Anti-*p*-cAbl (1:200 C5240; Sigma-Aldrich, USA) was used with the Biotin-Avidin peroxidase system previously prepared (ABC 1:100 LifeTechnologies 32020) in PBS. Slices were washed for 8 min with PBS, and stained using DAB substrate (ref. 11718096001; Roche) for 5–10 min. Finally, slices were washed with PBS and mounted with Entellan (Millipore 107960).

Electrophysiology—Acute hippocampal slices were prepared from 6 weeks old WT and c-Abl conditional knockout male littermates. Brain slices were cut at 400 μm thickness using a Leica Vibrotome VT1200 in ice-cold dissection solution (250 mM sucrose, 4 mM KCl, 2 mM $CaCl_2$, 7 mM $MgCl_2$, 1.25 mM $NaHPO_4$, 2 mM $NaHCO_3$, pH 7.4) bubbled with 95% CO_2 and 5% O_2. Slices were incubated for 1 h at RT in ACSF (124 mM NaCl, 4 mM KCl, 2 mM $CaCl_2$, 1.8 mM $MgCl_2$, 1.25 mM $NaHPO_4$, 2 mM $NaHCO_3$, pH 7.4) constantly bubbled with 95% CO_2 and 5% O_2. Extracellular field excitatory postsynaptic potentials (fEPSP) were elicited by 200 μs long current pulses in the Shaeffer's collateral fiber and recording in CA1 stratum radiatum with a differential AC Amplifier Model 1800 A-M Systems and digitally acquired by custom written routines in Igor Pro (Wavemetrics, USA). Glass pipettes were pulled from borosilicate tubing in a P-87 Puller (Sutter Instruments, Novato CA) having 1–2 MOhm resistance and filled with ACSF. Input-Output (I-O) relationships were obtained by plotting the slope of fEPSP in function of stimulus intensity. For each current injection three recordings were obtained and averaged. Data points were fitted with the following Boltzmann distribution: fEPSP_slope = max_slope/(1 + exp(−z*(I – I_50)/RT)), where I_50 is the current needed to obtain half of the maximal response, max_slope is the maximal slope obtained at saturation, and z is the slope factor. For each experiment values are fitted to Boltzmann distribution and slopes are normalized to the maximal value.

QUANTIFICATION AND STATISTICAL ANALYSIS

Animal experiments were analyzed with GraphPad Prism8 software after classification into the Racine's scale.[57,58] The raw data is in figshare.com/s/d460eb722b56b5075fcd. Apoptotic nuclei percentage was calculated as apoptotic/(apoptotic+non-apoptotic

cells)*100. Results were statistically compared by Fisher's exact test and animal survival by Long-rank (Mantel-Cox) test and Chisquare. Dendritic spines and NR2B clustering numbers were quantified per 10 μm dendrite length of 3–5 dendrites from each neuron using ImageJ. Genotype vs. treatment results were compared using two-way ANOVA, followed by Tukey's post hoc multiple comparison test. Pertinent specific analyses were performed and informed for each figure. Data is presented as mean ± standard error of the mean (SEM).

Supplementary Material

Refer to Web version on PubMed Central for supplementary material.

ACKNOWLEDGMENTS

We thank Dr. Anthony Koleske (Yale School of Medicine), who kindly donated the c-Abl-KO mice; the Advanced Microscopy Facility UMA-UC; and animal facility CIBEM-UC. This work was supported by ANID grants FONDECYT 1201668 and 1241503 (A.A.R.), FONDECYT 1190334 and 1230337 (S.Z.), and FONDEF ID21I10347 (A.A.R.); Millennium Science Initiative Program - ICN09_016/ICN 2021_045; and the intramural research program at the National Center for Advancing Translational Sciences, NIH (J.M.).

REFERENCES

1. Fisher RS, Acevedo C, Arzimanoglou A, Bogacz A, Cross JH, Elger CE, Engel J, Forsgren L, French JA, Glynn M, et al. (2014). ILAE Official Report: A practical clinical definition of epilepsy. Epilepsia 55, 475–482. 10.1111/epi.12550. [PubMed: 24730690]
2. Fiest KM, Sauro KM, Wiebe S, Patten SB, Kwon C-S, Dykeman J, Pringsheim T, Lorenzetti DL, and Jetté N (2017). Prevalence and incidence of epilepsy. Neurology 88, 296–303. 10.1212/WNL.0000000000003509. [PubMed: 27986877]
3. Kwan P, Schachter SC, and Brodie MJ (2011). Drug-Resistant Epilepsy. N. Engl. J. Med.England 365, 919–926. 10.1056/NEJMra1004418.
4. Brodie MJ, Barry SJE, Bamagous GA, Norrie JD, and Kwan P (2012). Patterns of treatment response in newly diagnosed epilepsy. Neurology 78, 1548–1554. 10.1212/WNL.0b013e3182563b19. [PubMed: 22573629]
5. Laxer KD, Trinka E, Hirsch LJ, Cendes F, Langfitt J, Delanty N, Resnick T, and Benbadis SR (2014). The consequences of refractory epilepsy and its treatment. Epilepsy Behav 37, 59–70. 10.1016/J.YEBEH.2014.05.031. [PubMed: 24980390]
6. Engel J (1996). Introduction to temporal lobe epilepsy. Epilepsy Res 26, 141–150. 10.1016/S0920-1211(96)00043-5. [PubMed: 8985696]
7. Fisher RS, Van Emde Boas W, Blume W, Elger C, Genton P, Lee P, and Engel J (2005). Epileptic seizures and epilepsy: definitions proposed by the International League Against Epilepsy (ILAE) and the International Bureau for Epilepsy (IBE). Epilepsia 46, 470–472. 10.1111/J.0013-9580.2005.66104.X. [PubMed: 15816939]
8. Shao LR, Habela CW, and Stafstrom CE (2019). Pediatric Epilepsy Mechanisms: Expanding the Paradigm of Excitation/Inhibition Imbalance. Children 6, 23. 10.3390/CHILDREN6020023. [PubMed: 30764523]
9. Sloviter RS, Bumanglag AV, Schwarcz R, and Frotscher M (2012). Abnormal Dentate Gyrus Network Circuitry in Temporal Lobe Epilepsy.
10. Wong M, and Guo D (2013). Dendritic spine pathology in epilepsy: cause or consequence? Neuroscience 251, 141–150. 10.1016/J.NEUROSCIENCE.2012.03.048. [PubMed: 22522469]
11. Busche MA, Eichhoff G, Adelsberger H, Abramowski D, Wiederhold KH, Haass C, Staufenbiel M, Konnerth A, and Garaschuk O (2008). Clusters of hyperactive neurons near amyloid plaques in a mouse model of Alzheimer's disease. Science 321, 1686–1689. 10.1126/SCIENCE.1162844. [PubMed: 18802001]

12. Spoleti E, La Barbera L, Cauzzi E, De Paolis ML, Saba L, Marino R, Sciamanna G, Di Lazzaro V, Keller F, Nobili A, et al. (2024). Dopamine neuron degeneration in the Ventral Tegmental Area causes hippocampal hyperexcitability in experimental Alzheimer's Disease. Mol. Psychiatry 10.1038/S41380-024-02408-9.

13. Aronica E, Van Vliet EA, Mayboroda OA, Troost D, da Silva FH, and Gorter JA (2000). Upregulation of metabotropic glutamate receptor subtype mGluR3 and mGluR5 in reactive astrocytes in a rat model of mesial temporal lobe epilepsy. Eur. J. Neurosci 12, 2333–2344. 10.1046/J.1460-9568.2000.00131.X. [PubMed: 10947812]

14. DeLorenzo RJ, Sun DA, and Deshpande LS (2005). Cellular mechanisms underlying acquired epilepsy: the calcium hypothesis of the induction and maintainance of epilepsy. Pharmacol. Ther 105, 229–266. 10.1016/J.PHARMTHERA.2004.10.004. [PubMed: 15737406]

15. Yi JH, and Hazell AS (2006). Excitotoxic mechanisms and the role of astrocytic glutamate transporters in traumatic brain injury. Neurochem. Int 48, 394–403. 10.1016/J.NEUINT.2005.12.001. [PubMed: 16473439]

16. Meldrum BS (1994). The role of glutamate in epilepsy and other CNS disorders. Neurology 44, S14–S23. [PubMed: 7970002]

17. Hardingham GE, and Bading H (2010). Synaptic versus extrasynaptic NMDA receptor signalling: implications for neurodegenerative disorders. Nat. Rev. Neurosci 11, 682–696. 10.1038/NRN2911. [PubMed: 20842175]

18. Lee YS, and Silva AJ (2009). The molecular and cellular biology of enhanced cognition. Nat. Rev. Neurosci 10, 126–140. 10.1038/NRN2572. [PubMed: 19153576]

19. Auzmendi J, González N, and Girardi E (2009). The NMDAR subunit NR2B expression is modified in hippocampus after repetitive seizures. Neurochem. Res 34, 819–826. 10.1007/S11064-008-9828-0. [PubMed: 18751892]

20. Frasca A, Aalbers M, Frigerio F, Fiordaliso F, Salio M, Gobbi M, Cagnotto A, Gardoni F, Battaglia GS, Hoogland G, et al. (2011). Misplaced NMDA receptors in epileptogenesis contribute to excitotoxicity. Neurobiol. Dis 43, 507–515. 10.1016/J.NBD.2011.04.024. [PubMed: 21575722]

21. Viviani B, Bartesaghi S, Gardoni F, Vezzani A, Behrens MM, Bartfai T, Binaglia M, Corsini E, Di Luca M, Galli CL, and Marinovich M (2003). Interleukin-1beta enhances NMDA receptor-mediated intracellular calcium increase through activation of the Src family of kinases. J. Neurosci 23, 8692–8700. 10.1523/JNEUROSCI.23-25-08692.2003. [PubMed: 14507968]

22. Camacho A, Montiel T, and Massieu L (2007). Sustained metabolic inhibition induces an increase in the content and phosphorylation of the NR2B subunit of N-methyl-D-aspartate receptors and a decrease in glutamate transport in the rat hippocampus in vivo. Neuroscience 145, 873–886. 10.1016/J.NEUROSCIENCE.2006.12.069. [PubMed: 17331654]

23. Knox R, Brennan-Minnella AM, Lu F, Yang D, Nakazawa T, Yamamoto T, Swanson RA, Ferriero DM, and Jiang X (2014). NR2B phosphorylation at tyrosine 1472 contributes to brain injury in a rodent model of neonatal hypoxia-ischemia. Stroke 45, 3040–3047. 10.1161/STROKEAHA.114.006170. [PubMed: 25158771]

24. Ladépêche L, Planagumà J, Thakur S, Suárez I, Hara M, Borbely JS, Sandoval A, Laparra-Cuervo L, Dalmau J, and Lakadamyali M (2018). NMDA Receptor Autoantibodies in Autoimmune Encephalitis Cause a Subunit-Specific Nanoscale Redistribution of NMDA Receptors. Cell Rep 23, 3759–3768. 10.1016/J.CELREP.2018.05.096. [PubMed: 29949761]

25. Kharbanda S, Ren R, Pandey P, Shafman TD, Feller SM, Weichselbaum RR, and Kufe DW (1995). Activation of the c-Abl tyrosine kinase in the stress response to DNA-damaging agents. Nature 376, 785–788. 10.1038/376785A0. [PubMed: 7651539]

26. Zandy NL, Playford M, and Pendergast AM (2007). Abl tyrosine kinases regulate cell-cell adhesion through Rho GTPases. Proc Natl Acad Sci USA 104, 17686–17691. 10.1073/PNAS.0703077104. [PubMed: 17965237]

27. González-Martín A, Moyano T, Gutiérrez DA, Carvajal FJ, Cerpa W, Hanley JG, Gutiérrez RA, and Álvarez AR (2021). c-Abl regulates a synaptic plasticity-related transcriptional program involved in memory and learning. Prog. Neurobiol 205. 10.1016/J.PNEURO-BIO.2021.102122.

28. Gutiérrez D, Chandía-Cristi A, Yáñez M, Zanlungo S, and Álvarez A (2023). c-Abl kinase at the crossroads of healthy synaptic remodeling and synaptic dysfunction in neurodegenerative diseases. Neural Regen Res 18, 237–243. 10.4103/1673-5374.346540. [PubMed: 35900397]
29. Schlatterer SD, Acker CM, and Davies P (2011). c-Abl in neurodegenerative disease. J. Mol. Neurosci 45, 445–452. 10.1007/S12031-011-9588-1. [PubMed: 21728062]
30. Gonfloni S, Maiani E, Di Bartolomeo C, Diederich M, and Cesareni G (2012). Oxidative Stress, DNA Damage, and c-Abl Signaling: At the Cross-road in Neurodegenerative Diseases? Int J. Cell Biol 2012. 10.1155/2012/683097.
31. Vargas LM, Cerpa W, Muñoz FJ, Zanlungo S, and Alvarez AR (2018). Amyloid-b oligomers synaptotoxicity: The emerging role of EphA4/c-Abl signaling in Alzheimer's disease. Biochim. Biophys. Acta. Mol. Basis Dis 1864, 1148–1159. 10.1016/J.BBADIS.2018.01.023. [PubMed: 29378302]
32. La Barbera L, Vedele F, Nobili A, Krashia P, Spoleti E, Latagliata EC, Cutuli D, Cauzzi E, Marino R, Viscomi MT, et al. (2021). Nilotinib restores memory function by preventing dopaminergic neuron degeneration in a mouse model of Alzheimer's Disease. Prog. Neurobiol 202. 10.1016/J.PNEUROBIO.2021.102031.
33. Motaln H, and Rogelj B (2023). The Role of c-Abl Tyrosine Kinase in Brain and Its Pathologies. Cells 12, 2041. 10.3390/CELLS12162041. [PubMed: 37626851]
34. Alvarez AR, Sandoval PC, Leal NR, Castro PU, and Kosik KS (2004). Activation of the neuronal c-Abl tyrosine kinase by amyloid-beta-peptide and reactive oxygen species. Neurobiol. Dis 17, 326–336. 10.1016/J.NBD.2004.06.007. [PubMed: 15474370]
35. Cancino GI, Toledo EM, Leal NR, Hernandez DE, Yévenes LF, Inestrosa NC, and Alvarez AR (2008). STI571 prevents apoptosis, tau phosphorylation and behavioural impairments induced by Alzheimer's beta-amyloid deposits. Brain. 131, 2425–2442. 10.1093/BRAIN/AWN125. [PubMed: 18559370]
36. Gutierrez DA, Vargas LM, Chandia-Cristi A, de la Fuente C, Leal N, and Alvarez AR (2019). c-Abl Deficiency Provides Synaptic Resiliency Against Aβ-Oligomers. Front. Cell. Neurosci 13, 526. 10.3389/fncel.2019.00526. [PubMed: 31849613]
37. León R, Gutiérrez DA, Pinto C, Morales C, de la Fuente C, Riquelme C, Cortés BI, González-Martin A, Chamorro D, Espinosa N, et al. (2023). c-Abl tyrosine kinase down-regulation as target for memory improvement in Alzheimer's disease. Front. Aging Neurosci 15, 1180987. 10.3389/FNAGI.2023.1180987. [PubMed: 37358955]
38. Jing Z, Caltagarone J, and Bowser R (2009). Altered subcellular distribution of c-Abl in Alzheimer's disease. J Alzheimers Dis 17, 409–422. 10.3233/JAD-2009-1062. [PubMed: 19363261]
39. Chen L, Wang Z, Tang B, Fang M, Li J, Chen G, and Wang X (2014). Altered expression of c-Abl in patients with epilepsy and in a rat model. Synapse 68, 306–316. 10.1002/SYN.21741. [PubMed: 24623669]
40. Singh S, and Singh TG (2023). Imatinib Attenuates Pentylenetetrazole Kindled and Pilocarpine Induced Recurrent Spontaneous Seizures in Mice. Neurochem. Res 48, 418–434. 10.1007/S11064-022-03758-Y. [PubMed: 36239857]
41. Goodsell DS (2006). The molecular perspective: c-Abl tyrosine kinase. Stem Cells 24, 209–210. 10.1634/STEMCELLS.2005-CSC1. [PubMed: 16449631]
42. Lindholm D, Pham DD, Cascone A, Eriksson O, Wennerberg K, and Saarma M (2016). c-Abl Inhibitors Enable Insights into the Pathophysiology and Neuroprotection in Parkinson's Disease. Front. Aging Neurosci 8, 254. 10.3389/FNAGI.2016.00254. [PubMed: 27833551]
43. Turner RS, Hebron ML, Lawler A, Mundel EE, Yusuf N, Starr JN, Anjum M, Pagan F, Torres-Yaghi Y, Shi W, et al. (2020). Nilotinib Effects on Safety, Tolerability, and Biomarkers in Alzheimer's Disease. Ann. Neurol 88, 183–194. 10.1002/ANA.25775. [PubMed: 32468646]
44. Simuni T, Fiske B, Merchant K, Coffey CS, Klingner E, Caspell-Garcia C, Lafontant DE, Matthews H, Wyse RK, Brundin P, et al. (2021). Efficacy of Nilotinib in Patients With Moderately Advanced Parkinson Disease: A Randomized Clinical Trial. JAMA Neurol 78, 312–320. 10.1001/JAMANEUROL.2020.4725. [PubMed: 33315105]

45. Pagan FL, Hebron ML, Wilmarth B, Torres-Yaghi Y, Lawler A, Mundel EE, Yusuf N, Starr NJ, Anjum M, Arellano J, et al. (2020). Nilotinib Effects on Safety, Tolerability, and Potential Biomarkers in Parkinson Disease: A Phase 2 Randomized Clinical Trial. JAMA Neurol 77, 309–317. 10.1001/JAMANEUROL.2019.4200. [PubMed: 31841599]
46. Pagan FL, Wilmarth B, Torres-Yaghi Y, Hebron ML, Mulki S, Ferrante D, Matar S, Ahn J, and Moussa C (2021). Long-Term Safety and Clinical Effects of Nilotinib in Parkinson's Disease. Mov. Disord 36, 740–749. 10.1002/MDS.28389. [PubMed: 33215762]
47. Greuber EK, Smith-Pearson P, Wang J, and Pendergast AM (2013). Role of ABL family kinases in cancer: from leukaemia to solid tumours. Nat. Rev. Cancer 13, 559–571. 10.1038/NRC3563. [PubMed: 23842646]
48. Wolff NC, Richardson JA, Egorin M, and Ilaria RL (2003). The CNS is a sanctuary for leukemic cells in mice receiving imatinib mesylate for Bcr/Abl-induced leukemia. Blood 101, 5010–5013. 10.1182/BLOOD-2002-10-3059. [PubMed: 12595307]
49. Aghel N, Delgado DH, and Lipton JH (2017). Cardiovascular toxicities of BCR-ABL tyrosine kinase inhibitors in chronic myeloid leukemia: preventive strategies and cardiovascular surveillance. Vasc. Health Risk Manag 13, 293–303. 10.2147/VHRM.S108874. [PubMed: 28831263]
50. Zukas AM, and Schiff D (2018). Neurological complications of new chemotherapy agents. Neuro. Oncol 20, 24–36. 10.1093/NEUONC/NOX115. [PubMed: 28992326]
51. Adrián FJ, Ding Q, Sim T, Velentza A, Sloan C, Liu Y, Zhang G, Hur W, Ding S, Manley P, et al. (2006). Allosteric inhibitors of Bcrabl-dependent cell proliferation. Nat. Chem. Biol 2, 95–102. 10.1038/NCHEMBIO760. [PubMed: 16415863]
52. Marín T, Dulcey AE, Campos F, de la Fuente C, Acuña M, Castro J, Pinto C, Yañez MJ, Cortez C, McGrath DW, et al. (2022). c-Abl Activation Linked to Autophagy-Lysosomal Dysfunction Contributes to Neurological Impairment in Niemann-Pick Type A Disease. Front. Cell Dev. Biol 10, 844297. 10.3389/FCELL.2022.844297. [PubMed: 35399514]
53. Müller L, Tokay T, Porath K, Köhling R, and Kirschstein T (2013). Enhanced NMDA receptor-dependent LTP in the epileptic CA1 area via upregulation of NR2B. Neurobiol. Dis 54, 183–193. 10.1016/J.NBD.2012.12.011. [PubMed: 23313317]
54. Müller M, Gähwiler BH, Rietschin L, and Thompson SM (1993). Reversible loss of dendritic spines and altered excitability after chronic epilepsy in hippocampal slice cultures. Proc Natl Acad Sci USA 90, 257–261. 10.1073/PNAS.90.1.257. [PubMed: 8093558]
55. Zha XM, Green SH, and Dailey ME (2005). Regulation of hippocampal synapse remodeling by epileptiform activity. Mol. Cell. Neurosci 29, 494–506. 10.1016/J.MCN.2005.04.007. [PubMed: 15953736]
56. Turski WA, Czuczwar SJ, Kleinrok Z, and Turski L (1983). Cholinomimetics produce seizures and brain damage in rats. Experientia 39, 1408–1411. 10.1007/BF01990130. [PubMed: 6140182]
57. Racine RJ (1972). Modification of seizure activity by electrical stimulation. II. Motor seizure. Electroencephalogr. Clin. Neurophysiol 32, 281–294. 10.1016/0013-4694(72)90177-0. [PubMed: 4110397]
58. Lüttjohann A, Fabene PF, and van Luijtelaar G (2009). A revised Racine's scale for PTZ-induced seizures in rats. Physiol. Behav 98, 579–586. 10.1016/J.PHYSBEH.2009.09.005. [PubMed: 19772866]
59. El-Hassar L, Esclapez M, and Bernard C (2007). Hyperexcitability of the CA1 hippocampal region during epileptogenesis. Epilepsia 48 (Suppl 5), 131–139. 10.1111/J.1528-1167.2007.01301.X. [PubMed: 17910593]
60. Navidhamidi M, Ghasemi M, and Mehranfard N (2017). Epilepsy-associated alterations in hippocampal excitability. Rev. Neurosci 28, 307–334. 10.1515/REVNEURO-2016-0059. [PubMed: 28099137]
61. Zhang J, Adrián FJ, Jahnke W, Cowan-Jacob SW, Li AG, Iacob RE, Sim T, Powers J, Dierks C, Sun F, et al. (2010). Targeting Bcr-Abl by combining allosteric with ATP-binding-site inhibitors. Nature 463, 501–506. 10.1038/NATURE08675. [PubMed: 20072125]
62. Saleh T, Rossi P, and Kalodimos CG (2017). Atomic view of the energy landscape in the allosteric regulation of Abl kinase. NatNat. Struct. Mol. Biol 24, 893–901. 10.1038/NSMB.3470.

63. Neville K, Parise RA, Thompson P, Aleksic A, Egorin MJ, Balis FM, McGuffey L, McCully C, Berg SL, and Blaney SM (2004). Plasma and cerebrospinal fluid pharmacokinetics of imatinib after administration to nonhuman primates. Clin. Cancer Res 10, 2525–2529. 10.1158/1078-0432.CCR-03-0155. [PubMed: 15073132]
64. Yang X, Huang Y, Crowson M, Li J, Maitland ML, and Lussier YA (2010). Kinase inhibition-related adverse events predicted from in vitro kinome and clinical trial data. J Biomed Inform 43, 376–384. 10.1016/J.JBI.2010.04.006. [PubMed: 20434586]
65. Martinez NJ, Asawa RR, Cyr MG, Zakharov A, Urban DJ, Roth JS, Wallgren E, Klumpp-Thomas C, Coussens NP, Rai G, et al. (2018). A widely-applicable high-throughput cellular thermal shift assay (CETSA) using split Nano Luciferase. Sci. Rep 8, 9472. 10.1038/S41598-018-27834-Y. [PubMed: 29930256]
66. Savitski MM, Reinhard FBM, Franken H, Werner T, Savitski MF, Eberhard D, Martinez Molina D, Jafari R, Dovega RB, Klaeger S, et al. (2014). Tracking cancer drugs in living cells by thermal profiling of the proteome. Science 346, 1255784. 10.1126/SCIENCE.1255784. [PubMed: 25278616]
67. Bhatt VS, Zeng D, Krieger I, Sacchettini JC, and Cho JH (2016). Binding Mechanism of the N-Terminal SH3 Domain of CrkII and Proline-Rich Motifs in cAbl. Biophys. J 110, 2630–2641. 10.1016/J.BPJ.2016.05.008. [PubMed: 27332121]
68. Manouze H, Ghestem A, Poillerat V, Bennis M, Ba-M'hamed S, Benoliel JJ, Becker C, and Bernard C (2019). Effects of Single Cage Housing on Stress, Cognitive, and Seizure Parameters in the Rat and Mouse Pilocarpine Models of Epilepsy. eNeuro 6. 10.1523/ENEURO.0179-18.2019.
69. Hadera MG, Eloqayli H, Jaradat S, Nehlig A, and Sonnewald U (2015). Astrocyte-neuronal interactions in epileptogenesis. J. Neurosci. Res 93, 1157–1164. 10.1002/JNR.23584. [PubMed: 25782696]
70. Lévesque M, and Avoli M (2013). The kainic acid model of temporal lobe epilepsy. Neurosci. Biobehav. Rev 37, 2887–2899. 10.1016/J.NEUBIOREV.2013.10.011. [PubMed: 24184743]
71. Younus I, and Reddy DS (2018). A resurging boom in new drugs for epilepsy and brain disorders. Expert Rev. Clin. Pharmacol 11, 27–45. 10.1080/17512433.2018.1386553. [PubMed: 28956955]
72. Nair AB, and Jacob S (2016). A simple practice guide for dose conversion between animals and human. J. Basic Clin. Pharm 7, 27–31. 10.4103/0976-0105.177703. [PubMed: 27057123]
73. Ahmed Juvale II, and Che Has AT (2020). The evolution of the pilocarpine animal model of status epilepticus. Heliyon 6, e04557. 10.1016/J.HELIYON.2020.E04557. [PubMed: 32775726]
74. Karuppagounder SS, Brahmachari S, Lee Y, Dawson VL, Dawson TM, and Ko HS (2014). The c-Abl inhibitor, nilotinib, protects dopaminergic neurons in a preclinical animal model of Parkinson's disease. Sci. Rep 4, 4874. 10.1038/SREP04874. [PubMed: 24786396]
75. During MJ, and Spencer DD (1993). Extracellular hippocampal glutamate and spontaneous seizure in the conscious human brain. Lancet 341, 1607–1610. 10.1016/0140-6736(93)90754-5. [PubMed: 8099987]
76. Kapur J (2018). Role of NMDA receptors in the pathophysiology and treatment of status epilepticus. Epilepsia Open 3, 165–168. 10.1002/EPI4.12270. [PubMed: 30564775]
77. Hanada T (2020). Ionotropic Glutamate Receptors in Epilepsy: A Review Focusing on AMPA and NMDA Receptors. Biomolecules 10, 464. 10.3390/BIOM10030464. [PubMed: 32197322]
78. Goldberg EM, and Coulter DA (2013). Mechanisms of epileptogenesis: a convergence on neural circuit dysfunction. Nat. Rev. Neurosci 14, 337–349. 10.1038/NRN3482. [PubMed: 23595016]
79. Salter MW, and Kalia LV (2004). Src kinases: a hub for NMDA receptor regulation. Nat. Rev. Neurosci 5, 317–328. 10.1038/NRN1368. [PubMed: 15034556]
80. Perez de Arce K, Varela-Nallar L, Farias O, Cifuentes A, Bull P, Couch BA, Koleske AJ, Inestrosa NC, and Alvarez AR (2010). Synaptic clustering of PSD-95 is regulated by c-Abl through tyrosine phosphorylation. J. Neurosci 30, 3728–3738. 10.1523/JNEUR-OSCI.2024-09.2010. [PubMed: 20220006]
81. Glover RT, Angiolieri M, Kelly S, Monaghan DT, Wang JY, Smithgall TE, and Buller AL (2000). Interaction of the N-methyl-D-aspartic acid receptor NR2D subunit with the c-Abl tyrosine kinase. J. Biol. Chem 275, 12725–12729. 10.1074/JBC.275.17.12725. [PubMed: 10777567]

82. Mossman T (1983). Rapid colorimetric assay for cellular growth and survival: application to proliferation and cytotoxicity assays. J. Immunol. Methods 65, 55–63. 10.1016/0022-1759(83)90303-4. [PubMed: 6606682]

83. Kaech S, and Banker G (2006). Culturing hippocampal neurons. Nat. Protoc 1, 2406–2415. 10.1038/NPROT.2006.356. [PubMed: 17406484]

Highlights

- Pilocarpine-induced status epilepticus (SE) produces c-Abl phosphorylation in mice brain
- c-Abl mediates NMDAR excitotoxicity in neurons and epilepsy
- Neurotinib administration improves survival and extends latency of pilocarpine-SE mice

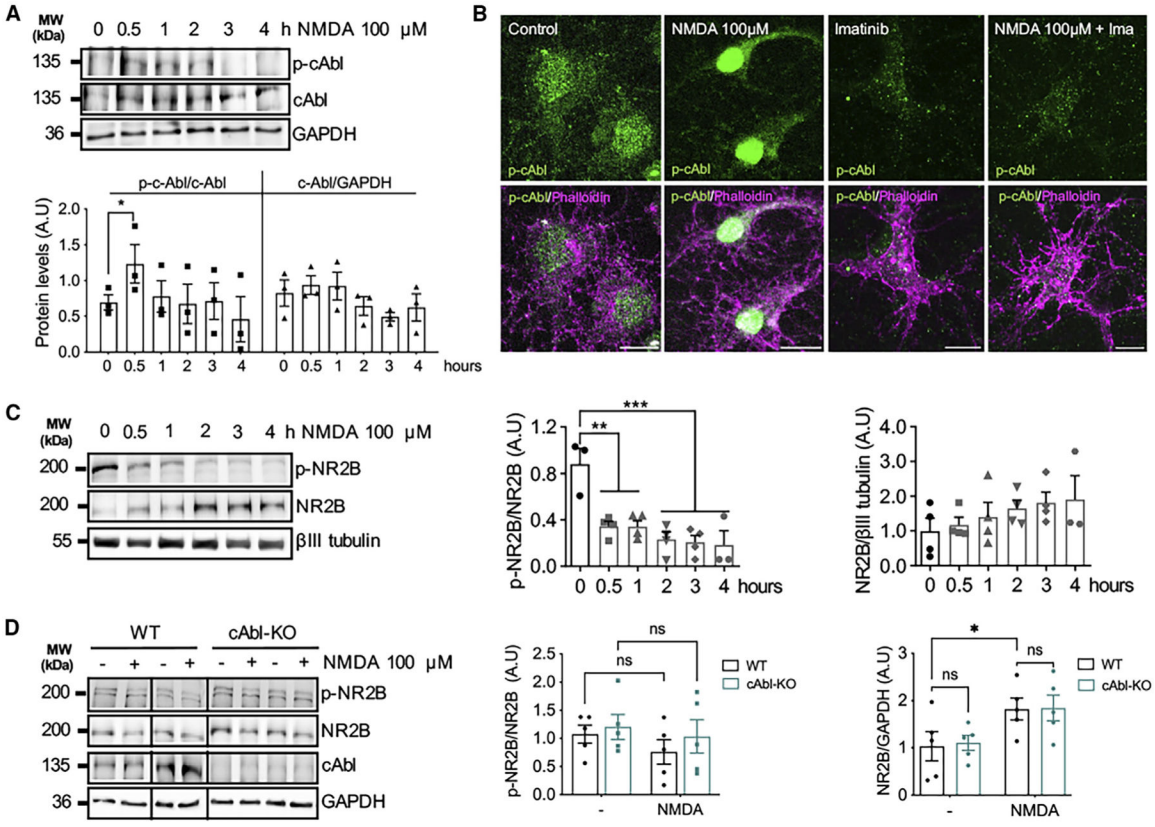

Figure 1. c-Abl tyrosine kinase activity is induced by NMDAR excitotoxicity in vitro

(A) Cortical neurons (10 days *in vitro* [DIV]) were treated with 100 µM NMDA for indicated time points. c-Abl phosphorylation Y412 (p-c-Abl) and total c-Abl were examined by western blot ($n = 3$, one-way ANOVA Kruskal-Wallis test).

(B) Hippocampal neurons (15 DIV) were treated with 100 µM NMDA with or without Ima 5 µM (c-Abl inhibitor) for 1 h. Immunofluorescence showing p-c-Abl (green) and phalloidin staining (magenta). Nuclear p-c-Abl signal (white arrows, Δ). Scale bar, 20 µm.

(C) Cortical neurons (10 DIV) were treated with 100 µM NMDA for indicated time points, and Y1472 (p-NR2B) and NR2B total levels were assessed by western blot. βIII tubulin used as loading control. Data represent p-NR2B protein levels normalized to NR2B total protein levels ($n = 3$, one-way ANOVA Tukey's test).

(D) Wild-type (WT) and c-Abl knockout (c-Abl-KO) cortical neurons (10 DIV) were treated with 100 µM NMDA for an hour of continuous exposure, and p-NR2B and total NR2B levels were analyzed by western blot. GAPDH was used as loading control. WT $n = 5$ and c-Abl-KO $n = 5$ embryos (two-way ANOVA p-NR2B $p = 0.3044$ and NR2B $^{**}p = 0.0073$ on NMDA treatment, $p = 0.8530$ genotype effect). Data are shown as mean ± SEM, and statistically significant differences are indicated: ns, non-significant; $^{*}p < 0.05$; $^{**}p < 0.01$; $^{***}p < 0.001$.

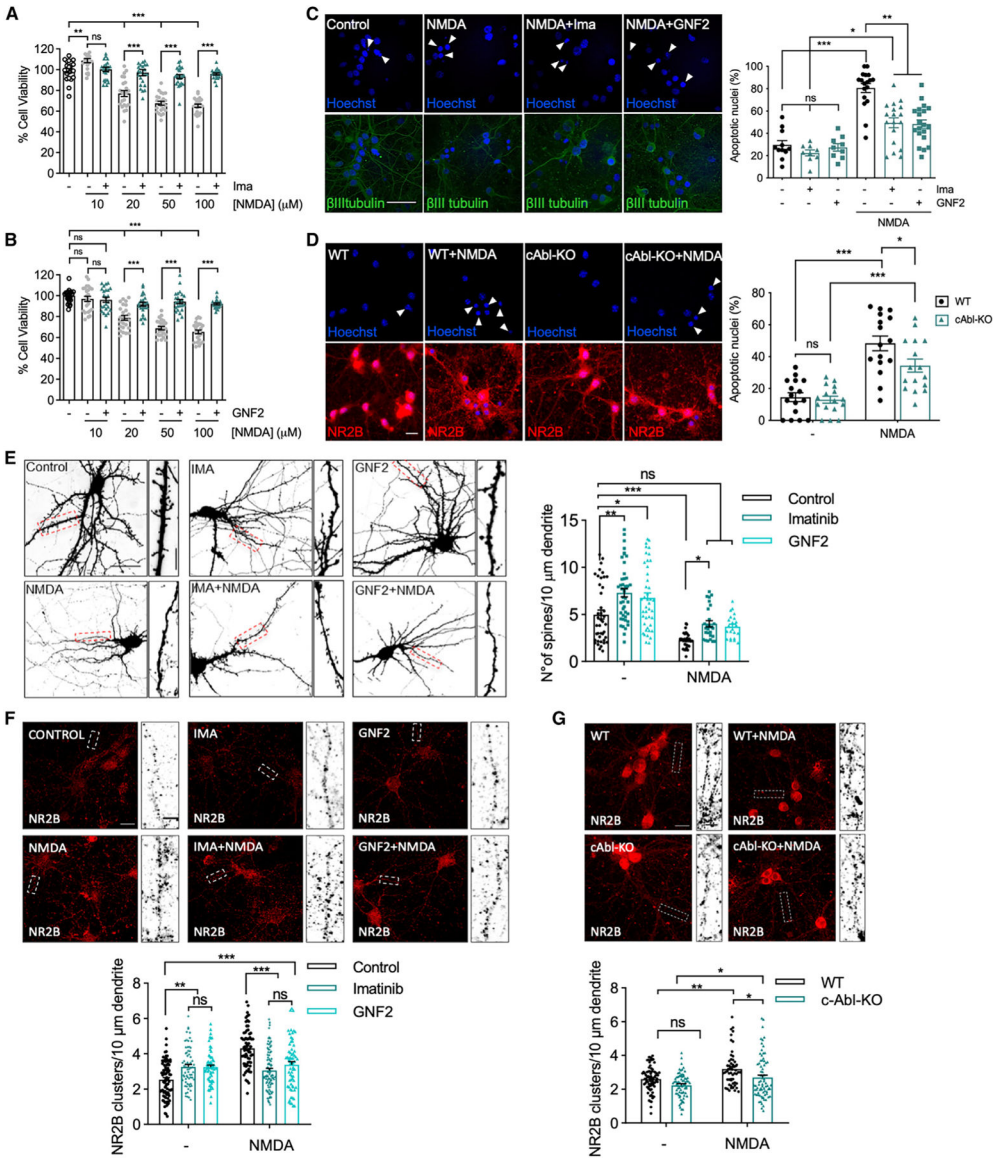

Figure 2. c-Abl inhibition or ablation prevents apoptosis, dendritic spine loss, and the increase in NR2B clustering induced by NMDAR excitotoxicity *in vitro*

(A and B) MTT cytotoxicity assays were performed using cortical neurons exposed to 10–100 μM NMDA plus 5 μM imatinib (Ima) (A) or 5 μM GNF2 (B) for 24 h ($n = 3$ different experiments, 24 replicates, Newman-Keuls test for non-repeated-measures one-way ANOVA).

(C and D) Immunofluorescence showing βIII tubulin (green) and Hoechst staining (blue) from hippocampal neurons (15 DIV) treated with 100 μM NMDA; (C) with or without Ima, or GNF2. Graph shows the percentage of apoptotic nuclei (white arrows, Δ) from $n = 3$ independent experiments, 20 images of 5–29 averaged neurons per image per condition; (D) WT and c-Abl-KO neurons. Graph shows the percentage of apoptotic nuclei (white arrows, Δ) from $n = 4$ WT and 4 c-Abl-KO embryos, 16 images of 5–19 averaged neurons per image per condition). Bonferroni test non-repeated-measures one-way ANOVA. Scale bar, 20 μm.

(E) GFP-expressing hippocampal neurons (15 DIV). After 48 h of transfection, neurons were treated with 100 μM NMDA for 1 h with or without Ima or GNF2. Scale bar, 20 μm and 5 μm for dendrite sections. Graph shows quantification of dendritic spines per 10-μm section of 3–5 dendrites for each neuron ($n = 3$ different experiments, 22–45 dendrites, two-way ANOVA Tukey's test).

(F and G) NR2B (red) immunofluorescence of hippocampal neurons (15 DIV); (F) treated with Ima or GNF2; (G) WT and c-Abl-KO neurons. White rectangles show gray-scale NR2B clusters in a dendrite section. Scale bar, 20 μm and 5 μm for magnifications. Graph shows quantification NR2B clusters along 10 μm of 3–5 dendrites for each neuron ($n = 3$ different experiments, 62–89 dendrites, two-way ANOVA, Tukey's test). Data are shown as mean ± SEM, statistically significant differences are indicated: $*p < 0.05$, $**p < 0.01$, $***p < 0.001$.

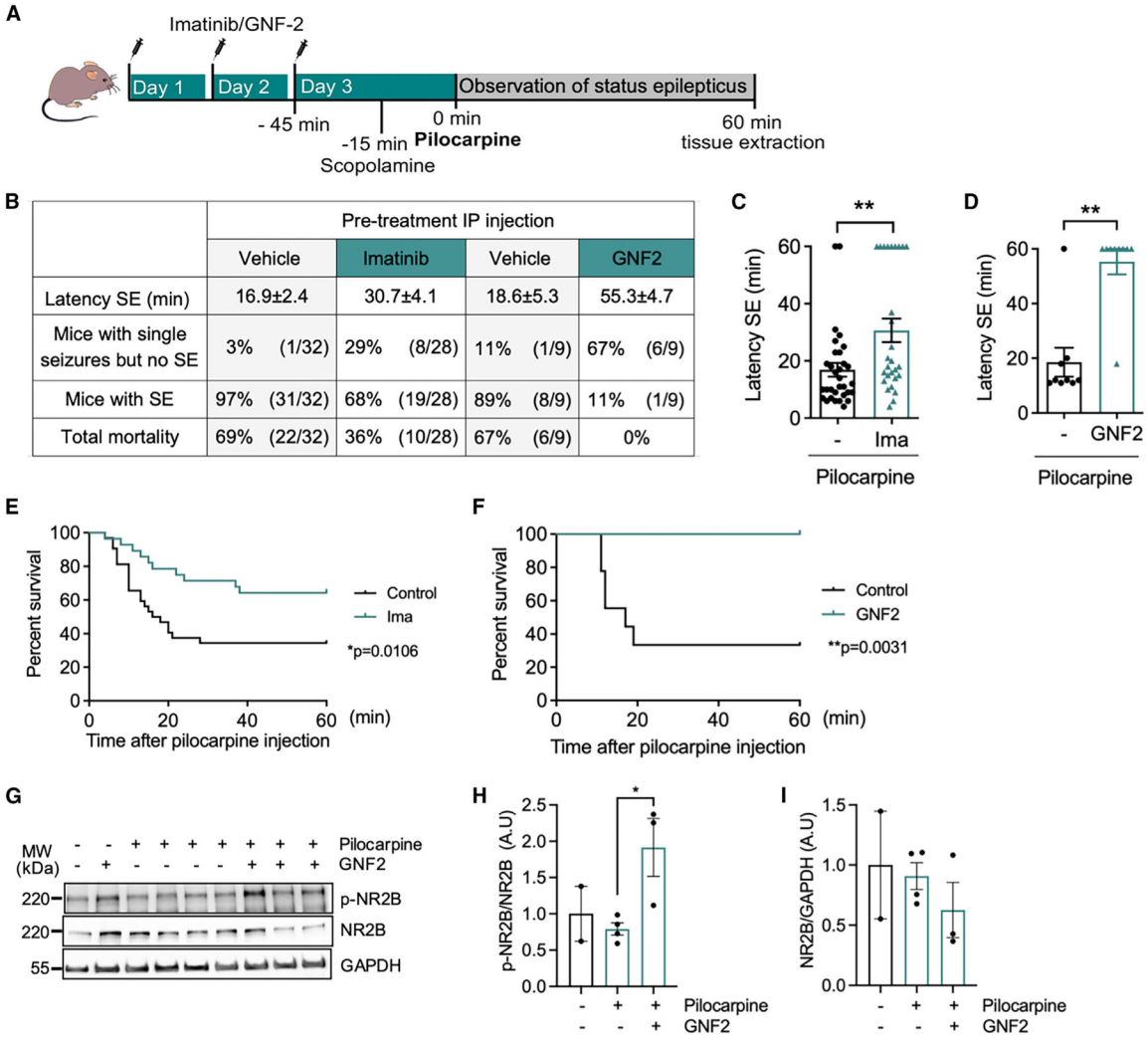

	Pre-treatment IP injection			
	Vehicle	Imatinib	Vehicle	GNF2
Latency SE (min)	16.9±2.4	30.7±4.1	18.6±5.3	55.3±4.7
Mice with single seizures but no SE	3% (1/32)	29% (8/28)	11% (1/9)	67% (6/9)
Mice with SE	97% (31/32)	68% (19/28)	89% (8/9)	11% (1/9)
Total mortality	69% (22/32)	36% (10/28)	67% (6/9)	0%

Figure 3. c-Abl inhibition by imatinib and GNF2 increases survival and diminishes seizure symptoms in pilocarpine-induced SE mice

(A–F) Mice were injected intraperitoneally (i.p.) with imatinib (Ima) 12.5 mg/kg (vehicle $n = 32$, Ima $n = 28$ mice) or GNF2 12.5 mg/kg (vehicle $n = 9$ and GNF2 $n = 9$ mice) for 3 days; 30 min after injecting Ima or GNF2 on the last day, animals were injected with scopolamine, and, 15 min after, convulsions were induced by i.p. injection of pilocarpine. Behavior and seizures were evaluated according to Racine's scale. SE, time to SE (latency to SE), and mice survival were recorded for 60 min post pilocarpine injection. Mice were sacrificed at the end of the experiment. (A) Experimental time line. (B) Table summarizes Ima- and GNF2-treated mice behavior after pilocarpine injection, the number and percentage of mice developing seizures without SE, SE (Racine scale ≥4), latency, and total mortality. (C and D) Graphs of latency to SE. (C) Latency vehicle = 16.9 ± 2.4 min and Ima = 30.7 ± 4.1 min, $^{**}p = 0.0087$ Mann-Whitney t test. (D) Latency vehicle = 18.6 ± 5.3 min and GNF2 = 55.3 ± 4.7 min, $^{**}p = 0.0012$ Mann-Whitney t test.(E and F) Percentage survival (E) Ima $^{*}p = 0.0106$, log rank test, chi square = 6.539; (F) GNF2 $^{**}p = 0.0031$, log rank test, chi square = 8.723.

(G–I) Hippocampal lysates from GNF2 or vehicle-injected mice prior to pilocarpine injection were analyzed by western blot (G). Quantification shows p-NR2B (H) and NR2B (I) total levels. βIII tubulin used as load control. n = 2–5 animals per condition, *post hoc* one-way ANOVA tests. $*p < 0.05$, $**p < 0.01$. Data are shown as mean ± SEM.

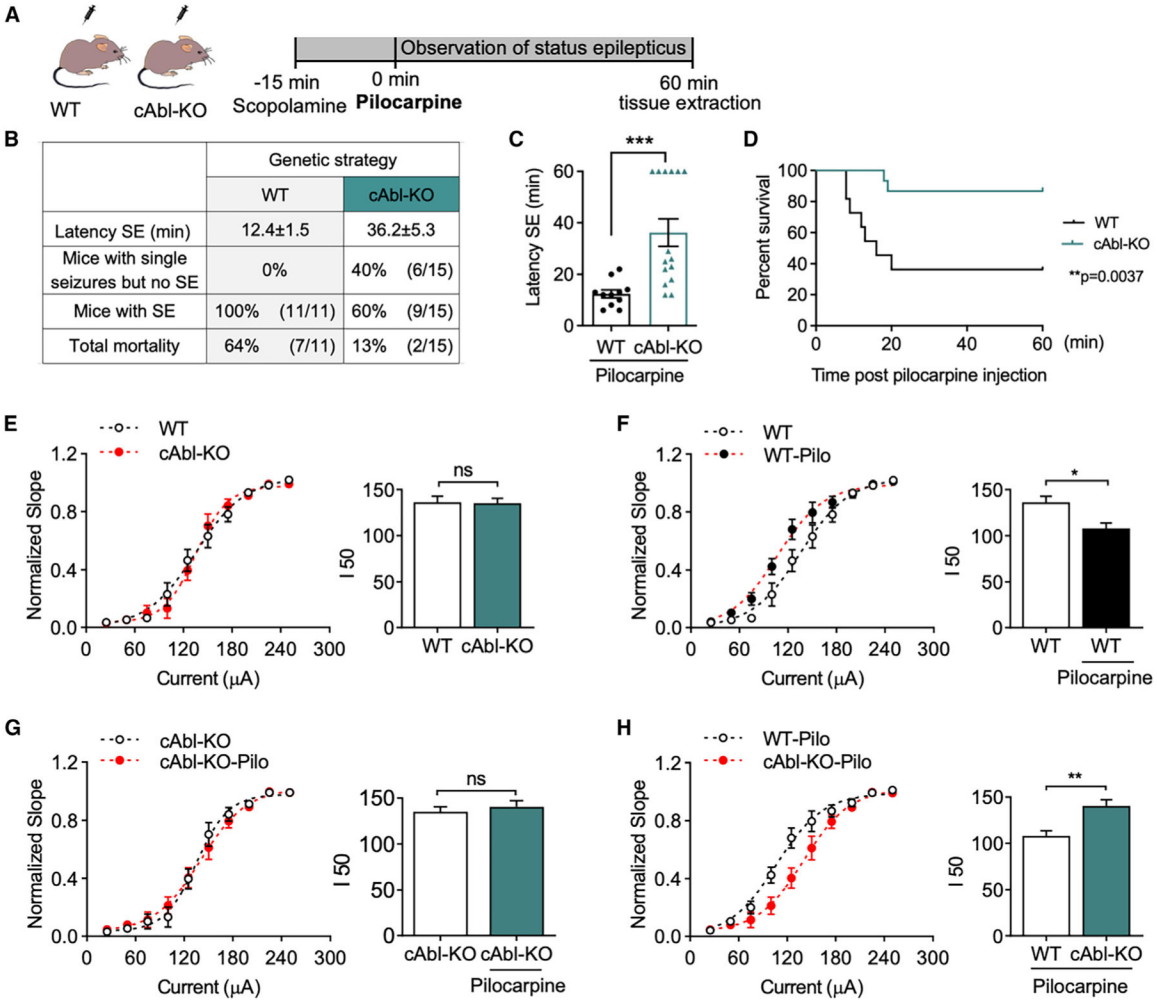

Figure 4. c-Abl null mice have diminished epileptic symptoms, improved survival, and no pilocarpine-induced increase in the hippocampi's circuit excitability

(A–D) WT (n = 10) and c-Abl-KO (n = 15) mice were injected i.p. with scopolamine, and, 15 min after, convulsions were induced with pilocarpine (A). Behavior and seizures were evaluated according to Racine's scale for 60 min post pilocarpine. (B) Table summarizes mice behavior after pilocarpine injection, the number of mice developing seizures without SE, SE, latency, and total mortality. (C) Graph of latency: WT = 12.4 ± 1.5, c-Abl-KO = 36.2 ± 5.3 min. Mann-Whitney t test ***$p < 0.001$. (D) Percentage survival **$p = 0.0037$, log rank test: chi square = 8.428.

(E–H) I-O relationships obtained from the slope of field excitatory postsynaptic potential (fEPSP) in response to current stimulation fEPSP were assessed in hippocampal slices of WT and c-Abl-KO mice injected with pilocarpine. To the right of each I-O curve is a bar plot with I_50 (midpoint) values obtained from Boltzmann fit. Data are shown as mean ± SEM.

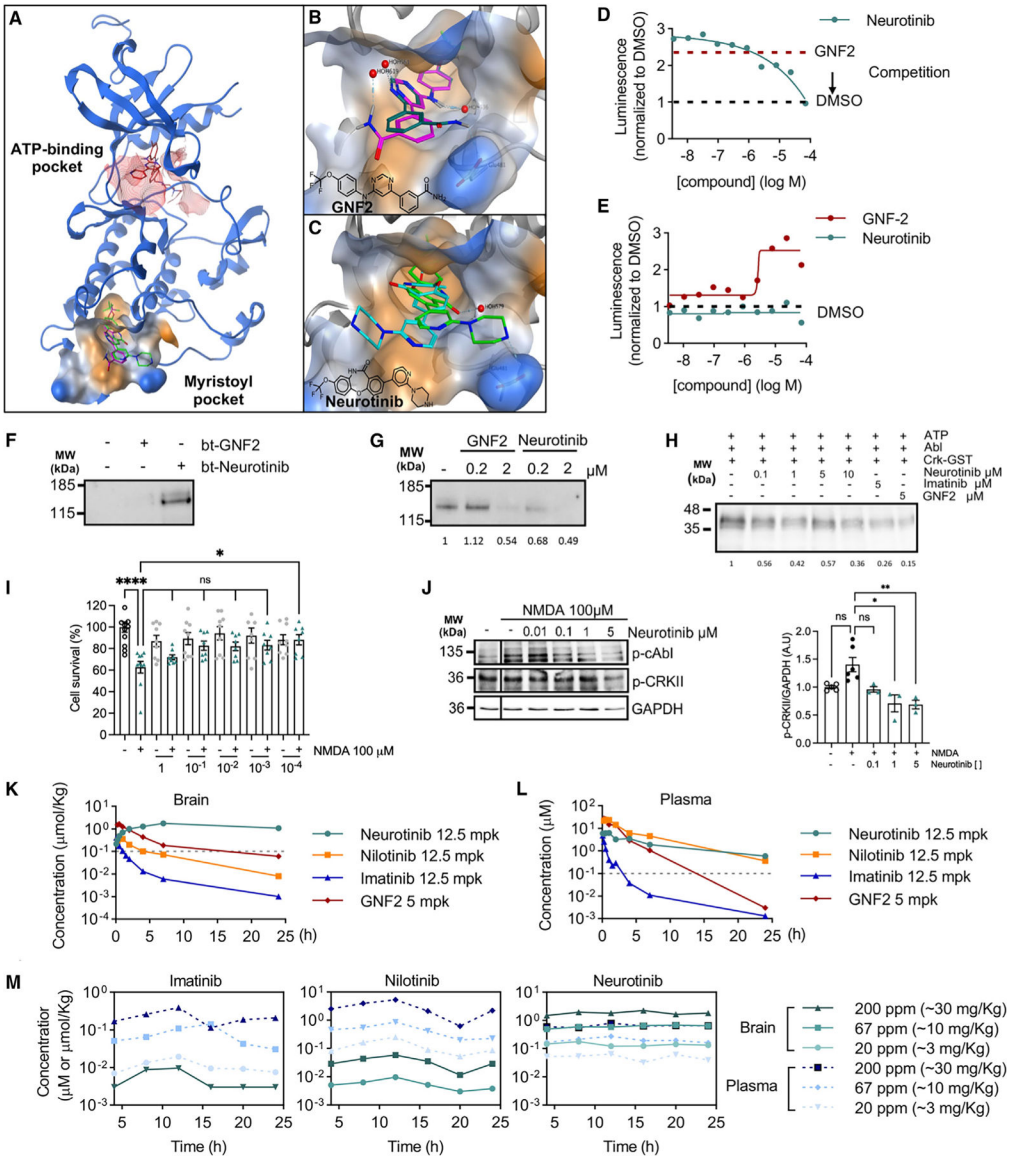

Figure 5. The new allosteric drug neurotinib binds to the myristoyl pocket of c-Abl and has improved brain penetrance in mice

(A) c-Abl structure (PDB: 3K5V) showing imatinib bound to the ATP-binding site (red mesh surface), allosteric modulators GNF2, and neurotinib bound to the myristoyl pocket (hydrophobic surface).

(B) Binding models of GNF2 predicted from docking. Above (carbon atoms, magenta): the amide group of GNF2 points to the left side (free energy [ΔG] = −8.22 kcal/mol) of the myristoyl pocket forming a water-mediated H-bond. A second water-mediated H-bond is formed in the inner pocket. Bottom (dark green): the amide group of GNF2 points to the right side (ΔG = −8.10 kcal/mol) forming an H-bond with Glu481.

(C) Binding models of neurotinib from docking studies. The predicted binding ΔG= −7.41 kcal/mol (left side, cyan) and ΔG= −8.37 kcal/mol (right side, green). In the right-side model, the pyridine group points out and forms an H-bond with Glu481, while the carbonyl group forms a water-mediated H-bond in the inner pocket.

(D and E) GNF2-induced thermal stabilization was measured using SplitLuc CETSA. Hek293 cells expressing the 86b-*c*-Abl kinase domain were treated with GNF2 (E, 30 μM) or neurotinib in 10-point dose-response prior to heating to 49°C for 3.5 min. Thermally stable protein was detected by luminescence.

(F) Biotinylated GNF2 or neurotinib were immobilized onto magnetic streptavidin Dynabeads to pull down the recombinant c-Abl protein. DMSO served as negative control. c-Abl retained on the beads was detected by an α-His tag immunoblot (left).

(G) Recombinant c-Abl was pre-mixed with GNF2 or neurotinib at 0.2 or 2 μM, and biotinylated GNF2 bound to streptavidin Dynabeads was pulled down.

(H) Phosphorylation of CRKII-GST substrate assessed by phosphotyrosine 4G10 immunoblot after the incubation with activated c-Abl obtained from 10 DIV cortical neurons treated for 15 min with 100 μM H_2O_2.

(I) Cortical neurons were treated with 100 μM NMDA plus neurotinib at different concentrations for 6 h. MTT cytotoxicity assays were performed (n = 3 independent experiments, four replicates each).

(J) Cortical neurons were treated with neurotinib (0.01–5 μM) plus 100 μM NMDA. p-c-Abl and CRKII Y221 phosphorylated (*p*-CRKII) levels were assessed by western blot. GAPDH was used as a load control (n = 3 independent experiments with replicates). One-way ANOVA Kruskal-Wallis test control vs. NMDA $p = 0.7864$.

(K and L) Pharmacokinetics of single-dose i.p. administration comparison between neurotinib, imatinib, GNF2, and nilotinib.

(M) Brain and plasma levels after 14-day administration of chow containing 20 ppm (3 mg/kg daily exposure), 67 ppm (10 mg/kg daily exposure), and 200 ppm (30 mg/kg daily exposure) of imatinib, neurotinib, or nilotinib.

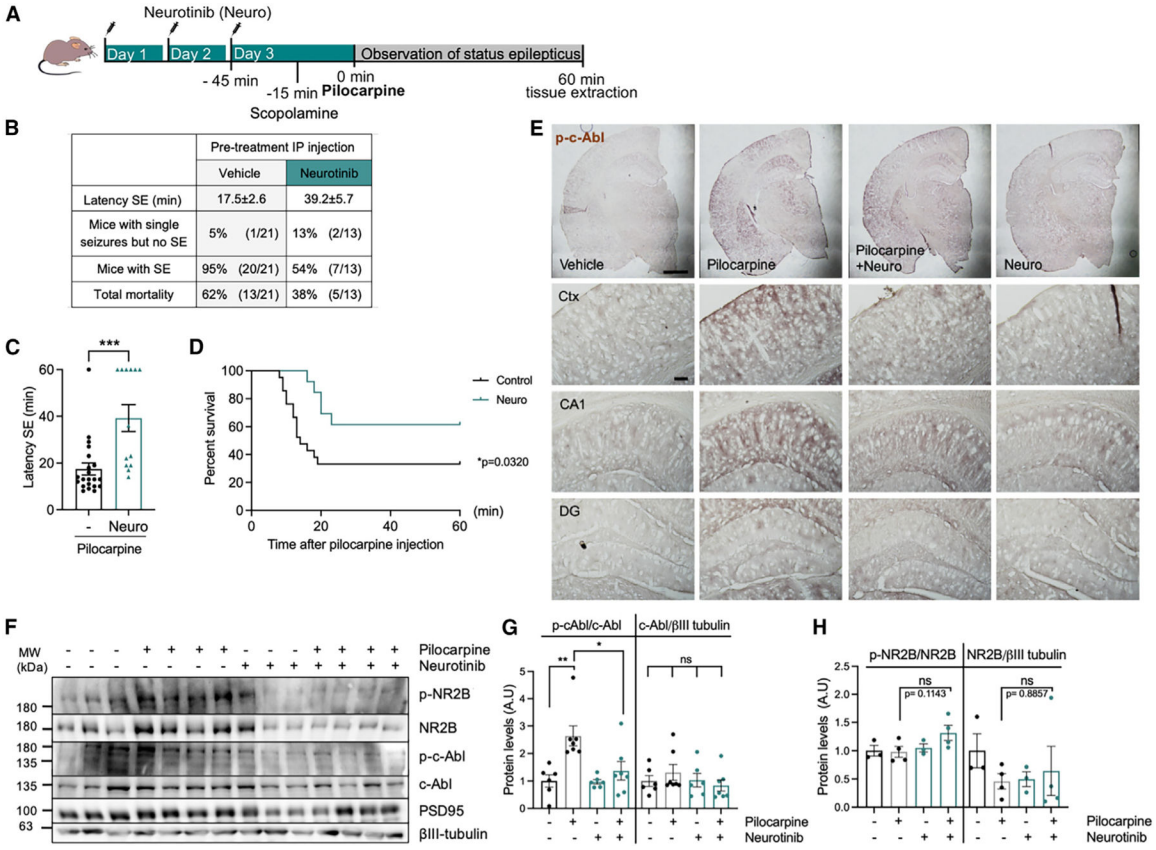

Figure 6. c-Abl-increased phosphorylation was inhibited with neurotinib, which improved survival and diminished seizure symptoms in pilocarpine-induced SE mice

(A–D) (A) Mice were i.p. injected with 5 mg/kg neurotinib (neuro) for 3 days and later with pilocarpine to induce SE (vehicle $n = 21$, neurotinib $n = 13$ mice). Behavior and seizures were evaluated according to Racine's scale for 60 min post pilocarpine injection and mice were sacrificed at the end of the experiment. (B) Table summarizes mice behavior after pilocarpine injection. (C) Graph of latency to SE; vehicle = 17 ± 2.6, neurotinib = 39.2 ± 5.7 min, Mann-Whitney t test ***$p = 0.0003$. (D) Percentage survival: vehicle vs. neurotinib *$p = 0.0320$ log rank test: chi square = 4.6, df = 1.

(E) p-c-Abl immunohistochemistry of brain slices (upper panel scale bar, 1 μm); hippocampus (CA3), cortex (Ctx), and dentate gyrus (DG) (brain sections scale bar, 100 μm). $n = 3$ animals.

(F–H) (F) p-c-Abl and c-Abl western blots of hippocampal lysates from neurotinib or vehicle i.p.-injected mice post-pilocarpine survival. βIII tubulin used as load control. (G) Quantification of p-c-Abl/c-Abl, n = 6–7 animals (one-way ANOVA, Tukey's test vehicle vs. pilocarpine **$p = 0.0032$, pilocarpine vs. neuro + pilocarpine *$p = 0.0191$) and c-Abl/βIII tubulin (one-way ANOVA Kruskal-Wallis test $p = 0.4878$). (H) Quantification of phosphorylated p-NR2Band NR2B total levels, n = 3–4 animals. p-NR2B/NR2B (one-way ANOVA, Mann-Whitney test $p = 0.1143$); and NR2B/βIII tubulin (one-way ANOVA, Mann-Whitney test $p = 0.8857$). Statistical differences are indicated: *$p < 0.05$, **$p < 0.01$. Data are shown as mean ± SEM.

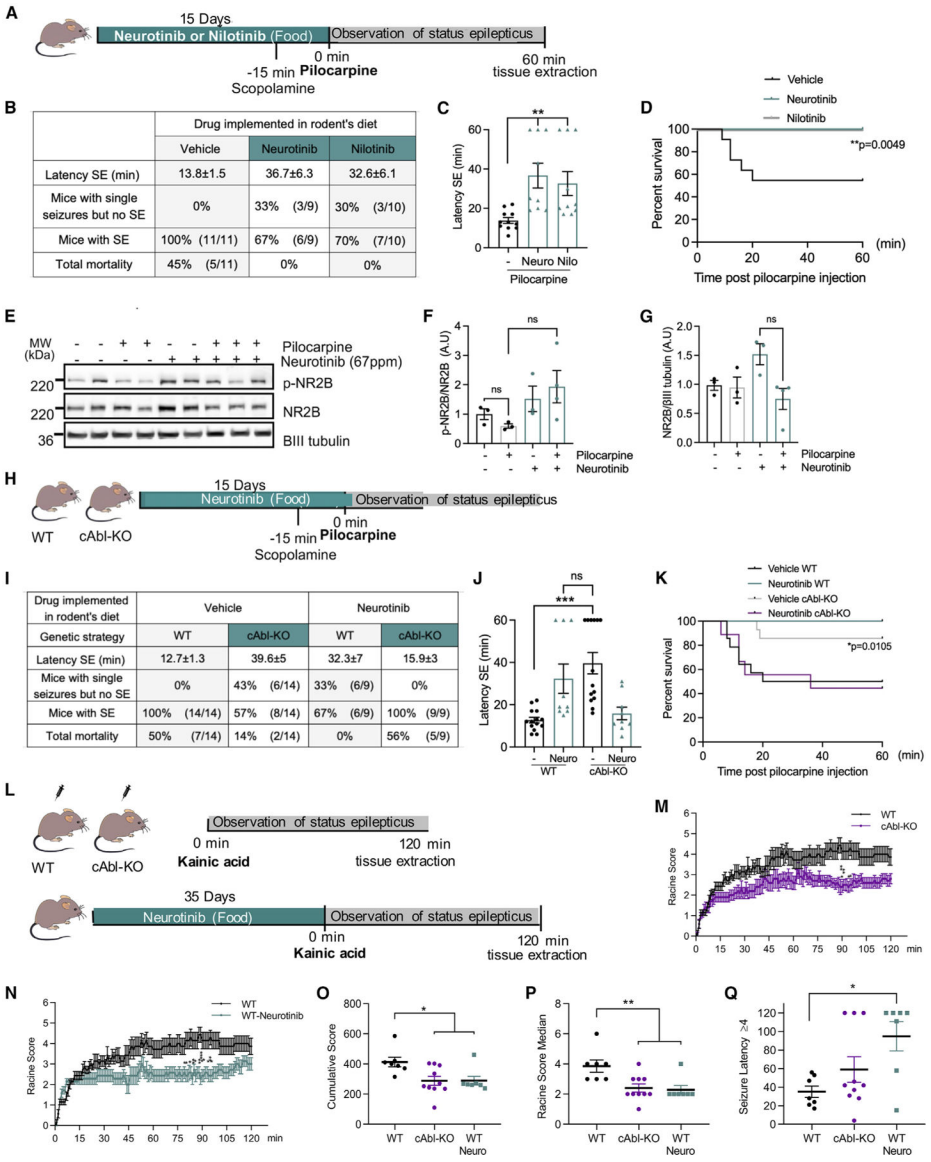

Figure 7. Neurotinib diet improved survival and increased latency in pilocarpine- and kainic-acid-injected SE mice, except in c-Abl-KO pilocarpine-induced-SE mice fed with neurotinib

(A) Mice fed with 67 ppm neurotinib diet or 200 ppm nilotinib diet for 2 weeks were induced to developed SE with pilocarpine (vehicle $n = 11$, neurotinib $n = 9$, and nilotinib $n = 10$ mice fed with each chow).

(B) Table summarizes mice behavior after pilocarpine injection.

(C) Latency to SE: vehicle = 13.8 ± 1.5, neurotinib chow = 36.7 ± 6.3, nilotinib chow = 32.6 ± 6.1 (one-way ANOVA Kruskal-Wallis test vehicle vs. neurotinib $^{**}p = 0.0011$, vehicle vs. nilotinib $^{**}p = 0.0059$).

(D) Percentage survival: vehicle vs. neuro/nilotinib chow $^{**}p = 0.0049$ log rank test, chi square = 10.63, df = 2.

(E–G) (E) Hippocampal lysates from mice fed with neurotinib or control diet were analyzed post pilocarpine injection survival. p-NR2B and NR2B total levels were assessed by western blot. βIII tubulin used as load control. (F) Quantification of p-NR2B/NR2B, one-way

ANOVA Kruskal-Wallis test pilocarpine vs. pilocarpine + neurotinib $p = 0.0759$. (G) Quantification of NR2B/βIII tubulin. n = 3–4 animals.

(H) WT and c-Abl-KO mice were fed with 67 ppm neurotinib for 2 weeks and induced to develop seizures with pilocarpine (WT-vehicle $n = 14$, WT + neurotinib $n = 14$, c-Abl-KO-vehicle $n = 9$, and c-Abl-KO + neurotinib $n = 9$ fed mice).

(I and J) (I) Table summarizes mice behavior after pilocarpine injection. (J) Latency to SE: WT + vehicle = 12.7 ± 1.3, c-Abl-KO + vehicle = 39.6 ± 5, WT + neurotinib = 32.3 ± 7, c-Abl-KO + neurotinib = 15.9 ± 3 min, two-way ANOVA WT vs. c-Abl-KO ***$p = 0.0008$, WT vs. WT + neurotinib ns = 0.0630, c-Abl-KO vs. c-Abl-KO + neurotinib *$p = 0.0266$, WT + neurotinib vs. c-Abl-KO + neurotinib ns = 0.2499.

(K) Percentage survival. All groups log rank test: chi square = 11.25 *$p = 0.0105$, df = 3.

(L) WT mice were fed with neurotinib diet for 35 days (67 ppm) to 8 weeks old, injected with kainic acid (KA), and their behavior scored with Racine's scale for 120-min recording. WT = 7, c-Abl-KO = 10, and WT mice fed with neurotinib = 7 (67 ppm). Mice were sacrificed at the end of the experiment.

(M) Average seizure score of KA-treated WT and c-Abl-KO mice (*$p < 0.05$, **$p < 0.01$, ***$p < 0.001$, two-way ANOVA, Sidak's test).

(N) Average seizure score of KA-treated WT and WT-neurotinib mice (*$p < 0.05$, **$p < 0.01$, ***$p < 0.001$, two-way ANOVA, Sidak's test).

(O) Responsiveness to KA of WT, c-Abl-KO, and WT mice fed with neurotinib. Accumulative score WT, 413 ± 32; c-Abl-KO, 290 ± 29; and WT-neurotinib, 288 ± 30 arbitrary units (*$p < 0.05$, one-way ANOVA, Tukey's test).

(P) Median scores for seizure activity during 2 h after KA injection. Racine score median WT, 3.86 ± 0.4; c-Abl-KO, 2.29 ± 0.29; and WT-neurotinib, 2.4 ± 0.27 (**$p < 0.01$, one-way, Tukey's test).

(Q) Latency to SEWT, 35.14 ± 6.17; c-Abl-KO, 94.86 ± 15.83; and WT-neurotinib, 59 ± 13.81 min (*$p < 0.05$, one-way ANOVA, Tukey's test). Data are shown as mean ± SEM.

KEY RESOURCES TABLE

REAGENT or RESOURCE	SOURCE	IDENTIFIER
Antibodies		
Mouse Anti-Phosphotyrosine Recombinant 4g10 Monoclonal antibody, Unconjugated, Clone 4g10	Millipore	Cat# 05–321, RRID:AB_309678
Mouse anti-*c*-Abl (24-11)	Santa Cruz Biotechnology	Cat# sc-23; RRID:AB_626775
Anti-GluN2B/NR2B Glutamate Receptor Antibody	Antibodies Incorporated	Cat# 75–101, RRID:AB_2232584
Phospho-NMDAR2B (Tyr1472) Polyclonal Antibody	Thermo Fisher Scientific	Cat# 38-7000; RRID:AB_2533379
Anti-phospho-*c*-Abl (pTyr412) antibody produced in rabbit	Sigma-Aldrich	Cat# C5240; RRID:AB_262088
Monoclonal Anti-*c*-Abl antibody produced in mouse	Sigma-Aldrich	Cat# A5844; RRID:AB_258262
Rabbit anti-phospho CRKII (Y221)	Cell Signaling Technology	Cat# 3491; RRID:AB_2229920
Mouse anti-GAPDH (6C5)	Santa Cruz Biotechnology	Cat# sc32233; RRID:AB_627679
Mouse anti-β3 Tubulin (2G10)	Santa Cruz Biotechnology	Cat# sc80005; RRID:AB_2210816
Mouse anti-GFAP monoclonal antibody, unconjugated, clone [GA5]	Cell Signaling Technology	Cat# 3670; RRID:AB_561049
anti-Iba1	Norvus Bio	Cat#NB-100-1028; RRID:AB_521594
Mouse anti-NeuN [EPR12763]	Abcam	Cat# ab177487, RRID:AB_2532109
Donkey anti-Mouse IgG (H + L) Highly Cross-Adsorbed Secondary Antibody, Alexa Fluor™ 488	ThermoFischer Scientific	Cat# A21202; RRID:AB_141607
Donkey anti-Mouse IgG (H + L) Highly Cross-Adsorbed Secondary Antibody, Alexa Fluor™ 555	ThermoFischer Scientific	Cat# A31570; RRID:AB_2536180
Goat anti-Mouse IgG (H + L) Cross-Adsorbed Secondary Antibody, Alexa Fluor™ 633	ThermoFischer Scientific	Cat# A21050; RRID:AB_2535718
Goat anti-Mouse IgG (H + L) Highly Cross-Adsorbed Secondary Antibody, Alexa Fluor™ 594	ThermoFischer Scientific	Cat# A11032; RRID:AB_2534091
anti-His tag	Invitrogen	Cat# MA1-21315
Goat anti-mouse IgG (H + L) Secondary antibody, HRP	ThermoFischer Scientific	Cat# 31430; RRID:AB_228307
Goat anti-rabbit IgG (H + L) Secondary antibody, HRP	ThermoFischer Scientific	Cat# 31460; RRID:AB_228341
Biological samples		
Primary culture cortical and hippocampal neurons from rat and mouse	Laboratory of Alejandra Álvarez, PUC, Chile	N/A
Rat and mouse brain	CIBEM, PUC	N/A
Chemicals, peptides, and recombinant proteins		
Pilocarpine Hydrochloride	Sigma-Aldrich	P6503
Scopolamine Methyl Nitrate	Sigma-Aldrich	S2250
Diazepam	Sigma-Aldrich	D0899
Kainic acid	Laboratory of Andres Dulcey, NIH, USA	N/A
Neurotinib (inhibitor)	Laboratory of Andres Dulcey, NIH, USA	Patent number WO2019/173761 A1
Imatinib mesylate (inhibitor)	Sigma-Aldrich	SML1027
GNF2 (inhibitor)	Sigma-Aldrich	G9420
L-glutamic acid (glutamate)	Sigma-Aldrich	G2128

REAGENT or RESOURCE	SOURCE	IDENTIFIER
NMDA	Tocris	Cat 0114
Global 18% protein rodent diet 2018	Envigo/Teklad	N/A
NIH-31 Open Formula Mouse/Rat Sterilizabile Diet	7017	N/A
3-[4,5-dimethylthiazol-2-yl]-2,5-diphenyltetrazolium bromide	Sigma-Aldrich	M6494
Protein G Agarose	Santa Cruz Biotechnology	sc2002
ATP disodium salt hydrate	Sigma-Aldrich	A2383
Hoechst 33342 staining	ThermoFisher Scientific	62249
c-Abl protein	ThermoFisher Scientific	PR4348B
Rhodamine-phalloidin	Invitrogen, Life Technologies	R415
M-280 Streptavidin Dynabeads	Invitrogen	11205D
N,N-Dimethylformamide	Merck	103053
NeutrAvidin-coupled agarose beads	Thermo Scientific	29200
ATP	Sigma-Aldrich	A26209
Biotin-Avidin peroxidase ABC 1:100	LifeTechnologies	32020
DAB substrate	Roche	Ref. 11718096001
Cytosine arabinoside	Sigma-Aldrich	147-94-4
Critical commercial assays		
Pierce™ BCA Protein Assay Kits	ThermoFisher Scientific	23227
InFusion reagents	Takara	
ECL substrate for detection of HRP enzyme activity	Thermo Scientific	32106
DirectPCR lysis reagent (EAR)	Viagen Biotech	401-E
Biotin-Avidin peroxidase ABC 1:100	LifeTechnologies	32020
Magnetofection (Neuromag transfection reagent)	Oz Biosciences	NM50200
Deposited data		
Raw data and PDB docking	This paper	http://figshare.com/s/d460eb722b56b5075fcd
Experimental models: Cell lines		
Human: K562 cells	ATCC	ATCC: CCL-243
Human: HEK293	ATCC	Cat# CRL-1573; RRID:CVCL_0045
Experimental models: Organisms/strains		
B6.129S4-Abl1tm1Ajk/J mice	Anthony Koleske donation	RRID:IMSR_JAX:024286
B6.Cg-Tg(Nes-cre)1Kln/J mice	Jackson laboratory	RRID:IMSR_JAX:003771
C56BL/6J mice	Jackson Laboratory	RRID:IMSR_JAX:000664
Sprague-Dawley rat	CIBEM-UC	RRID:MGI:5651135
Oligonucleotides		
Primers WT-Fw: TTGCTAAAGCGCTACATAGGA	Invitrogen	N/A
Primers Common: GCCTTATTGTGGAAGGACTG	Invitrogen	N/A

REAGENT or RESOURCE	SOURCE	IDENTIFIER
Primers Tg-Fw: CCTTCCTGAAGCAGTAGAGCA	Invitrogen	N/A
Recombinant DNA		
pGEX-CRK-SH2	gift from Bruce Mayer	Addgene plasmid #46418; RRID:Addgene_46418; http://n2t.net/addgene:46418
pcDNA3-EGFP	gift from Doug Golenbock	Addgene plasmid#13031; RRID:Addgene_13031; http://n2t.net/addgene:13031
c-Abl-86b fusion protein backbone (RefSeq: NP_005148.2)	This paper, Eurofins, Martínez et al., 2018[48]	N/A
Software and algorithms		
ImageJ	Schneider et al. 201282	https://imagej.nih.gov/ij/
GraphPad Prism 8	GraphPad Software	https://www.graphpad.com
Other		
AC Amplifier Model 1800	A-M Systems	https://www.a-msystems.com/p-253-model-1800-2-channel-microelectrode-ac-amplifier.aspx
Glass pipette P-87 Puller	Sutter Instruments, Novato CA	N/A
Eclipse C2 Ti-E confocal microscope	Nikon	N/A
ViewLux microplate reader	PerkinElmer	https://resources.perkinelmer.com/corporate/content/relatedmaterials/brochures/bro_viewluxpicturethis.pdf
Cryostat CM1850	Leica	https://www.leicabiosystems.com/sites/default/files/media_product-download/2022-05/Leica_CM1850_UV_IFU_1v5C_en.pdf
Bioanalysis in Column: HALO 2.7mm Biphenyl 90A (50*2.1 mm)	Pharmaron	https://www.pharmaron.com
Bioanalysis in AB API 6500+ QTRAP LC/MS/MS instrument	SeqGen, Pharmaron	Serial N° CG20061507PL
Bioanalysis in HPLC: DGU-20A5R, Serial N° L20705312113 IX; LC-30AD Serial N° L20555407237 AE and L20555407239 AE; SIL-30AC, Serial N° L20565303416 AE), Rack Changer II (Serial N° L20585300808 SS; CTO-30A: Serial N° L20575300964 CD); CBM-20A: Serial N° L20235327682CD	Shimadzu, Pharmaron	N/A